Responses of Floating Wind Turbines to Wind and Wave Excitation

by

Kwang Hyun Lee

B.S.E. in Naval Architecture and Marine Engineering (1998)
University of Michigan

Submitted to the Department of Ocean Engineering
in partial fulfillment of the requirements for the degree of

Master of Science in Ocean Engineering

at the
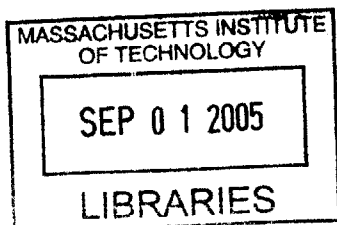
MASSACHUSETTS INSTITUTE OF TECHNOLOGY

January 2005

Author ....
Department of Ocean Engineering
January 10, 2004

Certified by ....
Paul D. Sclavounos
Professor of Naval Architecture
Thesis Supervisor

Accepted by ....
Michael S. Triantafyllou
Chairman, Departmental Committee on Graduate Students
Department of Ocean Engineering

BARKER

Responses of Floating Wind Turbines to Wind and Wave Excitation

by

Kwang Hyun Lee

Submitted to the Department of Ocean Engineering
on January 10, 2005, in partial fulfillment of the
requirements for the degree of
Master of Science in Ocean Engineering

Abstract

The use of wind power has recently emerged as a promising alternative to conventional electricity generation. However, space requirements and public pressure to place unsightly wind turbines out of visual range make it desirable to move large wind farms offshore and into deeper coastal waters. A necessary step for the deployment of wind turbines into deeper waters is the development of floating platform systems.

This thesis will present a general technical description of two concept designs for floating wind turbine systems, and make a preliminary evaluation of their performance in wind and waves. A new approach to computing the nonlinear wave excitation is also presented.

Thesis Supervisor: Paul D. Sclavounos
Title: Professor of Naval Architecture

Acknowledgments

Contents

List of Figures

List of Tables

List of Symbols

a	: axial flow induction factor
A	: incident wave amplitude
$\mathbf{A}$	: added mass matrix
A_d	: area of the actuator disk
A_{ij}	: added mass coefficients
A_{WP}	: waterplane area
a_1	: parameter determining the speed of the wave front
a_2	: parameter affecting the steepness of the wave front
b	: breadth/height of the radial arm cross-section
$\mathbf{B}$	: damping matrix
$B_{ij,AERO}$	: aerodynamic damping coefficients
$B_{ij,WAVE}$	: wave damping coefficients
$\mathbf{C}$	: restoring matrix
C_D	: drag coefficient of a 2-D circular cylinder
$C_{D,square}$	: drag coefficient of a square
C_{ij}	: restoring coefficients
$C_{ij,HI}$	: hydrostatic + inertial restoring coefficients
$C_{ij,LINES}$	: restoring coefficients due to lines (subscript (*ZERO OFFSET*) indicates restoring coefficients at the zero offset position)
d	: diameter of floating platform
EA	: structural stiffness
g	: gravitational acceleration
H_s	: significant wave height
$\mathbf{I}$	: identity matrix
k	: wavenumber
L	: length of the radial arm
$\mathbf{M}$	: mass matrix
M	: mass of the floating wind turbine
M_{ij}	: mass coefficients
P	: a coefficient in the particle evolution equation
Q	: a coefficient in the particle evolution equation
r	: platform radius
R	: a coefficient in the particle evolution equation
RAO_j	: response amplitude operator in the jth mode of motion
S_ζ	: ambient wave spectrum
S_j	: spectrum of the response in the jth mode of motion
T	: platform draft
T_p	: peak period
T_0	: wind turbine thrust
u	: Eulerian fluid velocity in the x-direction
U	: wind speed at the location of the rotor disk
$\bar{U}$	: mean wind speed
U_{Stokes}	: Stokes drift velocity
V	: submerged volume of the floating wind turbine

V_g	: wave group velocity
w	: Eulerian fluid velocity in the z-direction
x_0	: location of vertical circular cylinder
$\mathbf{X}$	: hydrodynamic excitation
$\dot{x}$	: velocity of the wind turbine at the center of the rotor disk
$\mathbb{X}_j$	: complex amplitude of the hydrodynamic excitation
X_j	: hydrodynamic excitation in the jth mode of motion
$X_{i,AERO}$	: aerodynamic force or moment in the ith direction
$\overline{X}_{i,AERO}$	: mean aerodynamic force or moment in the ith direction
$X_{i,VISCOUS}$	: viscous drag force or moment in the ith direction
z_B	: z-coordinate of the center of buoyancy
z_d	: z-coordinate of the center of the rotor disk
z_F	: z-coordinate of the fairlead
z_G	: z-coordinate of the center of gravity
β	: wind/wave direction
γ	: gamma factor
ω	: wave frequency
ω_i	: natural frequency in the ith mode of motion
η	: instantaneous vector position of a fluid particle on the free surface
η_1	: instantaneous horizontal position of a fluid particle on the free surface
η_3	: instantaneous vertical position of a fluid particle on the free surface
ξ	: floating wind turbine response
ξ_j	: floating wind turbine response in the jth mode of motion
Ξ_j	: complex amplitude of the floating wind turbine response
$\xi_{j,STATIC}$	: mean offset position in static equilibrium
ρ	: density of water
ρ_{AIR}	: density of air
$\rho_{CONCRETE}$	: density of concrete
σ_j	: RMS response in the jth mode of motion
ζ	: wave elevation

Chapter 1

Introduction

The use of wind power has recently emerged as a promising alternative to conventional electricity generation. However, space requirements and public pressure to place unsightly wind turbines out of visual range make it desirable to move large wind farms offshore and into deeper coastal waters. A necessary step for the deployment of wind turbines into deeper waters (50 – 300 meter depth) is the development of floating platform systems.

This thesis will present a general technical description of two concept designs for floating wind turbine systems, and examine their performance in wind and waves. A new approach to computing the nonlinear wave excitation is also presented.

1.1   Offshore Wind Farms

There are several reasons why an offshore location for wind farms may be desirable. A few of the more important reasons are listed below:

- Environmental and economic considerations
- Fewer space constraints
- Generally higher and steadier wind velocities
- Allowance for higher tip speed designs (for increased efficiency), as acoustic requirements are less important offshore
- Proximity to densely populated coastal cities (load centers)

Additionally, there are several reasons to design floating wind turbines, as opposed to the currently existing steel monopiles or conventional gravity bases:

- Ability to move wind farms further offshore to avoid visual intrusiveness
- Flexibility in positioning individual wind turbines, due to the relative insensitivity to water depth and seabed conditions (Tong, 1998)
- Reduced complexity in construction and installation

1.2   Overview of Engineering

The entire floating wind turbine system has been modeled as a rigid body and only the case of steady wind loading has been considered. However, it is proposed that such a preliminary study will provide a good basis for further work – particularly in the design of floating platforms and mooring system configurations.

The SWIM-MOTIONS-LINES (SML) suite of programs has been used for several of the calculations in this thesis. In particular, the SWIM module was used to carry out the linear frequency-domain analysis for the floating platforms, while the LINES module was used to compute the static tension in the mooring lines and the linear restoring (stiffness) matrices. The SML suite is the result of a ten-year research and development effort at the Massachusetts Institute of Technology funded by the oil industry, and it has been extensively validated through collaboration with project sponsors. The principal advantage of using SWIM for the hydrodynamic calculations in this thesis is that analytic solutions for basic geometries have been used, such as those for truncated vertical circular cylinders, horizontal pontoons, and slender rods. This circumvents the need for time-consuming computational procedures such as panel methods.

Finally, it should be mentioned that the features of the proposed floating platform designs represent currently existing technologies. The SPAR buoy, the tension-leg platform, and the taut-leg mooring system have all been successfully implemented by the offshore oil industry. What distinguishes the floating wind turbine from traditional offshore structures is the challenge of supporting an above-waterline structure with an unusually high center of gravity.

Chapter 2

General Technical Description of Proposed Designs

2.1   Introduction

A general technical description of two concept designs for floating platform systems will be presented. Each system will support a 1.5 MW wind turbine.

2.2   Above-waterline Structure

The principal characteristics of the 1.5 MW wind turbine (tower and tower-top structure) are as follows (see Figure 2-1):

- Shaft height = 84.00 m
- Rotor diameter = 70.00 m
- 3 blades

Figure 2-1: 1.5 MW wind turbine (tower and tower-top structure)

2.3   Floating Platform: *Design #1a*

2.3.1   Principal Characteristics

Design #1a has the following characteristics:

- Cylindrical floating buoy of draft $T = 15$ m and radius $r = 6$ m
- 3 radial arms of length = 20 m, breadth = 2 m, and height = 2 m
- Tension-leg mooring system with 3 lines (see Figure 2-2)
- Radial distance of lines from the vertical axis of the platform = 26 m
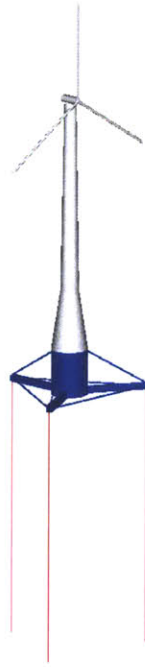- Water depth = 100 m

Figure 2-2: Floating wind turbine system (*Design #1a*) and mooring arrangement (*blue* denotes the wetted surface of the floating structure)

The characteristics of the lines are as follows:

> Fairlead Tension (N): 0.2007E+07
> Fairlead Angle (deg): 90.00 (with respect to the horizontal plane)
> Anchor Tension (N): 0.1944E+07
> Anchor Angle (deg): 90.00 (with respect to the horizontal plane)
> Unstretched length of lines = 84.89 m
> Material: Wire rope
> Diameter = 0.15 m
> Structural stiffness, EA = 1.5E+09 N (337,213 kips)
> Weight of line per unit length (in air) = 900 N/m (0.062 kips/feet)

The total system (floating platform and above-waterline structure) has a mass of M = 1,371 tonnes, which includes 532 tonnes of water ballast. The internal water ballast tank structure is compartmentalized such that free surface effects (sloshing) will be mitigated. The center of gravity of the ballasted structure is z_G = −2.92 m. The coordinate axes are defined in Figure 2-3.

2.3.2 Anchoring System

The resulting static vertical force upon each of the three anchors is 437 kips at an angle of 90.00 degrees to the sea bottom. The type of anchor normally used for tension-leg mooring systems is the TLP tendon pile. Other possibilities include the deadweight anchor and the embedment anchor (McCormick *et al.*, 1979).

2.3.3 Stability and Natural Frequencies

The present concept is found to be statically and dynamically stable (see Appendix A for an explanation of the stability criteria).

The natural frequencies are estimated by the solution of the complex eigenvalue problem obtained from the equations of motion after setting the exciting forces and moments equal to zero. The effect of linear damping is neglected and the added mass matrix is approximated by its zero-frequency value. The restoring component due to the mooring lines is evaluated about a zero mean offset. The modes of motion are defined in Figure 2-3.
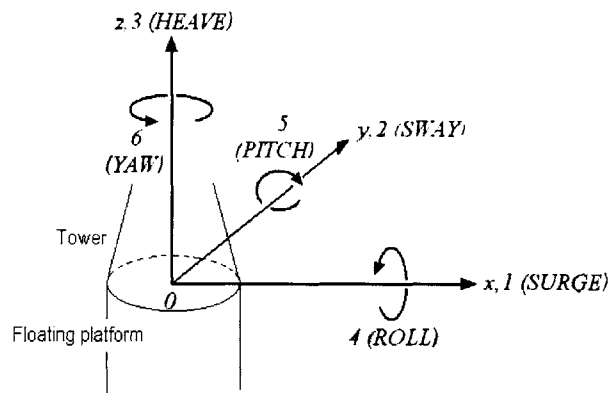

Figure 2-3: Definition of coordinate system and modes of motion

The natural frequencies of the system (at its zero mean offset position) are as follows:

$$\omega_1 = 0.13 \text{ rad/s}$$
$$\omega_2 = 0.13 \text{ rad/s}$$
$$\omega_3 = 5.29 \text{ rad/s}$$
$$\omega_4 = 3.94 \text{ rad/s}$$
$$\omega_5 = 3.94 \text{ rad/s}$$
$$\omega_6 = 0.45 \text{ rad/s}$$

2.4 Floating Platform: *Design #2a*

2.4.1 Principal Characteristics

Design #2a has the following characteristics:

13

- Cylindrical floating buoy of draft $T = 20$ m and radius $r = 6$ m
- Taut-leg mooring system with fairlead locations at $z_F = -20.0$ m and $z_F = 0.0$ m (at the waterline) as shown in Figure 2-4
- Radial distance of anchors from the vertical axis of the platform = 106 m
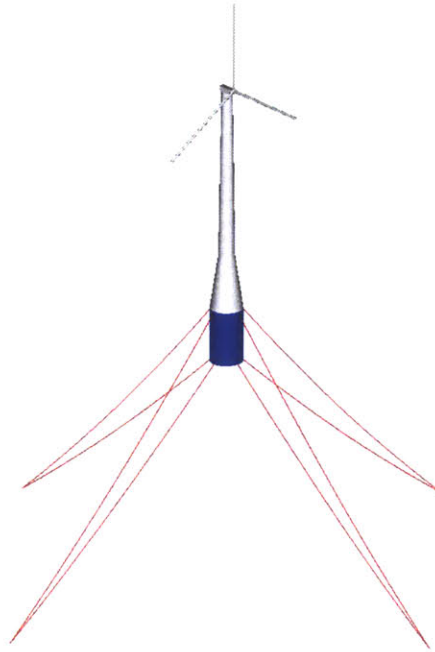- Water depth = 100 m

Figure 2-4: Floating wind turbine system (*Design #2a*) and mooring arrangement (*blue* denotes the wetted surface of the floating structure)

The characteristics of the lines are as follows:

- Lines with fairlead location $z_F = -20.0$ m:
    Fairlead Tension (N): 0.6168E+06
    Fairlead Angle (deg): 42.21
    Anchor Tension (N): 0.5568E+06
    Anchor Angle (deg): 34.86
    Unstretched length of lines = 128.10 m
- Lines with fairlead location $z_F = 0.0$ m:
    Fairlead Tension (N): 0.5506E+06
    Fairlead Angle (deg): 49.00
    Anchor Tension (N): 0.4756E+06
    Anchor Angle (deg): 40.59
    Unstretched length of lines = 141.5 m
- Mooring line properties:
    Material: Wire rope
    Diameter = 0.15 m

Structural stiffness, EA = 1.5E+09 N (337,213 kips)

Weight of line per unit length (in air) = 900 N/m (0.062 kips/feet)

The total system (floating platform and above-waterline structure) has a mass of M = 1,980 tonnes, which includes 1,569 tonnes of water ballast. The center of gravity of the ballasted structure is z_G = –5.74 m.

2.4.2 Anchoring System

The resulting force upon each of the four anchors is 1.0311E+06 N (231.8 kips) at an angle of 37.50 degrees to the sea bottom.

The traditional drag embedded anchor is not suitable for offshore wind turbine application, which requires precise location with no creep (Musial *et al.*, 2004). One possible (and cost-effective) solution for a taut-leg moored system is the embedded anchor plate, which can be precisely located and is not likely to creep over time. While anchor holding capacity data on embedded anchor plates is not available at present, an estimate of the range of possible anchor holding capacities may be made from data published for drag embedded anchors in the American Petroleum Institute's design manuals for offshore structures.

The required anchor holding capacity for the present case is 231.8 kips. This falls well within the range of the anchor holding capacities for existing drag embedded anchors – *i.e.*, 30 - 2,000 kips in soft clay and approximately 50 - 2,000 kips in sand.

2.3.3 Stability and Natural Frequencies

The present concept is found to be statically and dynamically stable. The natural frequencies of the system (at its zero mean offset position) are as follows:

$$\omega_1 = 1.16 \text{ rad/s}$$
$$\omega_2 = 1.16 \text{ rad/s}$$
$$\omega_3 = 2.09 \text{ rad/s}$$
$$\omega_4 = 0.91 \text{ rad/s}$$
$$\omega_5 = 0.91 \text{ rad/s}$$
$$\omega_6 = 0.79 \text{ rad/s}$$

2.5 Construction and Transportation to Installation Site

The floating wind turbines will be fully assembled at a shipyard and be transported to the offshore wind farm by tow. In order to ensure static stability while in tow, it is necessary to attach a concrete mass disk to the bottom surface of the floating structure (see Figure 2-5), in addition to filling the ballast tanks to capacity.

15

For the case of *Design #1a*, the properties of the mass disk are as follows:

Material: Concrete with density, $\rho_{CONCRETE} = 2,000 \, \text{kg/m}^3$
Radius = 6 m
Height = 1.55 m

In the towed condition, the floating wind turbine has a draft of 30.64 m, with 14.09 m of the tower submerged.
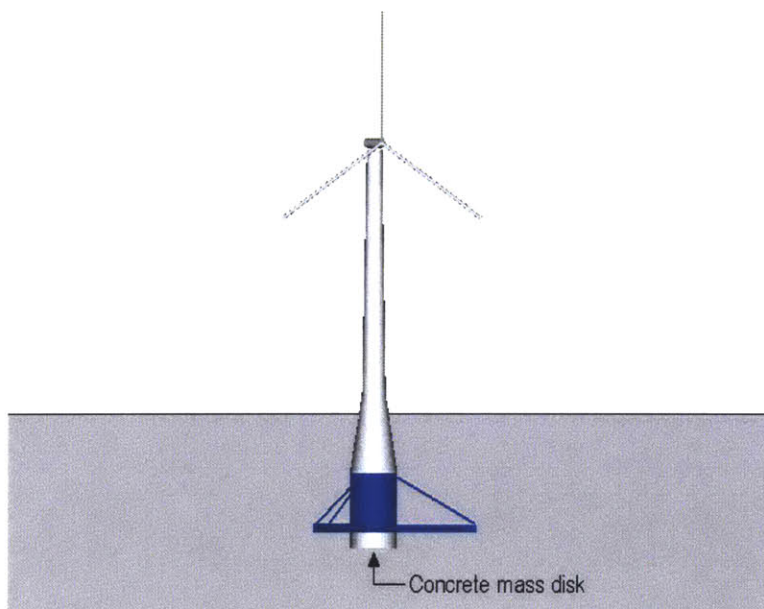
For the case of *Design #2a*, the properties of the mass disk are as follows:

Material: Concrete with density, $\rho_{CONCRETE} = 2,000 \, \text{kg/m}^3$
Radius = 6 m
Height = 2.21 m

In the towed condition, the floating wind turbine has a draft of 32.15 m, with 9.94 m of the tower submerged.

Figure 2-5: Floating wind turbine in the towed condition

Once at the installation site, the anchoring system is deployed and the mass disk is removed. The floating platform is then gradually de-ballasted while winches located inside the platform control the tensions on the lines to ensure static stability.

Chapter 3

Evaluation of Performance in Random Seas: A Linear Seakeeping Analysis

3.1 Introduction

The equations of motion for the floating wind turbine are as follows:

$$(\mathbf{M} + \mathbf{A})\ddot{\xi} + \mathbf{B}\dot{\xi} + \mathbf{C}\xi = \mathbf{X}(t) \qquad (3.1)$$

where $\mathbf{M}$ is the mass matrix, $\mathbf{A}$ is the added mass matrix, $\mathbf{B}$ is the linear damping matrix, $\mathbf{C}$ is the restoring matrix, $\mathbf{X}$ is the hydrodynamic excitation, and ξ is the floating wind turbine displacement from its mean offset position, where $\xi \in \mathbb{R}^6$ and $\mathbf{M}, \mathbf{A}, \mathbf{B}$, and $\mathbf{C}$ are 6×6 matrices.

For purposes of evaluating the performance of the proposed designs in random seas of arbitrary direction, a linear frequency-domain analysis is performed. The exciting forces and moments due to a plane progressive wave upon a floating wind turbine located at $(x, y) = (0,0)$ will be assumed to be of the form

$$X_j(t) = \mathrm{Re}\left\{\mathcal{X}_j(\omega)e^{i\omega t}\right\}, \quad j = 1, \ldots, 6 \qquad (3.2)$$

The response to such wave excitation, by virtue of linearity, will be of the form

$$\xi_j(t) = \mathrm{Re}\left\{\Xi_j(\omega)e^{i\omega t}\right\}, \quad j = 1, \ldots, 6 \qquad (3.3)$$

where both $\mathcal{X}_j(\omega)$ and $\Xi_j(\omega)$ are complex quantities.

3.2 Method of Analysis

3.2.1 Calculation of the Response Amplitude Operator

The principal seakeeping quantity from a linear seakeeping analysis of a floating body at zero speed is the Response Amplitude Operator (RAO). The RAO is defined as follows:

$$RAO_j(\omega) = \frac{\Xi_j(\omega)}{A/r^n}, \quad j = 1, \ldots, 6 \qquad (3.4)$$

where A is the incident wave amplitude, r is the radius of the platform, and $n = 0$ for $j = 1, 2, 3$ and $n = 1$ for $j = 4, 5, 6$.

The RAOs are found by solving the equations of motion for the system in the frequency-domain,

$$\left[-\omega^2 \left(M_{ij} + A_{ij}(\omega) \right) + i\omega B_{ij}(\omega) + C_{ij} \right] \Xi_j(\omega) = X_i(\omega) \tag{3.5}$$

3.2.2 Calculation of Coefficients and Excitation

The linear restoring matrix C_{ij} is composed of the following:

$$C_{ij} = C_{ij,HI} + C_{ij,LINES} \tag{3.6}$$

where $C_{ij,HI}$ is the hydrostatic + inertial restoring component and $C_{ij,LINES}$ is the restoring component due to the mooring lines.

The hydrostatic and inertial restoring coefficients are given by

$$C_{33,HI} = \rho g A_{WP}$$
$$C_{44,HI} = C_{55,HI} = \rho g V z_B - M g z_G + \rho g \iint_{A_{WP}} x^2 ds \tag{3.7}$$

where A_{WP} is the waterplane area, V is the submerged volume, and z_B is the location of the center of buoyancy.

The component due to the mooring lines, $C_{ij,LINES}$, is generated by the LINES module of the SWIM-MOTION-LINES (SML) suite of programs developed at MIT. The $C_{ij,LINES}$ matrix is evaluated at the mean offset position of the structure, which is caused by the mean aerodynamic loading, $\overline{X}_{i,AERO}$, on the turbine. The mean offset (or static equilibrium) position is found as follows:

$$\left[C_{ij,HI} + C_{ij,LINES(ZERO\ OFFSET)} \right] \xi_{j,STATIC} = \overline{X}_{i,AERO} \tag{3.8}$$

It is important to evaluate the restoring matrix due to the mooring lines about the mean offset position rather than the zero offset position. The strong nonlinearity of the force-displacement relationship of the mooring system for large mean offsets alters appreciably the structure of the $C_{ij,LINES}$ matrix (Kim and Sclavounos 2001).

The damping matrix B_{ij} is composed of a wave damping component $B_{ij,WAVE}(\omega)$, an aerodynamic component $B_{ij,AERO}$ (i.e., damping due to the aerodynamic loading upon the rotor), and an equivalent linear viscous damping component due to the floating platform.

18

The viscous damping due to the mooring lines is a relatively small quantity and it is neglected in the present study.

The module SWIM solves the linear radiation-diffraction problem for the given platform geometry by analytical techniques, generating $A_{ij}(\omega)$, $B_{ij,WAVE}(\omega)$ and $X_i(\omega)$. SWIM also computes the linear equivalent viscous damping due to the platform. The approximation of the steady wind loading and the aerodynamic damping matrix is described in Appendix B.

The program SWIM accepts as inputs the geometrical and inertial properties of the floating wind turbine, in addition to all external inputs generated by LINES. It then computes the RAOs of the system at the specified wave headings.

3.3   Responses of Floating Wind Turbines to Random Seas

3.3.1   Ambient Wave Spectrum

For a given ambient wave spectrum, $S_\zeta(\omega)$, the spectrum of the response may be found by the Wiener-Khinchine Relations:

$$S_j(\omega) = |RAO_j(\omega)|^2 S_\zeta(\omega), \qquad j = 1,2,3$$
$$S_j(\omega) = \left(|RAO_j(\omega)|/r\right)^2 S_\zeta(\omega), \quad j = 4,5,6$$

(3.9)

The ambient wave spectrum selected for this study is the JONSWAP spectrum, which is defined by the significant wave height H_s, the peak period T_p, and the gamma factor γ.

The variance of the response may then be found from the relation

$$\sigma_j^2 = \int_0^\infty S_j(\omega)d\omega$$

(3.10)

3.3.2   Environmental States

The responses of the floating wind turbines are calculated for long-crested seas at a wind/wave heading (defined in Figure 3-1) of $\beta = 45$ degrees for the following environmental states, which represent a range from *light* to *severe* weather conditions.

(1) mean wind speed of $\bar{U} = 5$ knots, and fully developed seas of significant wave height $H_s = 0.09$ m and $T_p = 2.0$ s ($\gamma = 1$)

(2) mean wind speed of $\bar{U} = 12$ knots, and fully developed seas of significant wave height $H_s = 0.67$ m and $T_p = 4.8$ s ($\gamma = 1$)

(3) mean wind speed of $\bar{U}$ = 20 knots, and fully developed seas of significant wave height H_s = 2.44 m and T_p = 8.1 s (γ = 1)

(4) mean wind speed of $\bar{U}$ = 28 knots, and fully developed seas of significant wave height H_s = 5.49 m and T_p = 11.3 s (γ = 1)

(5) mean wind speed of $\bar{U}$ = 40 knots, and fully developed seas of significant wave height H_s = 13.72 m and T_p = 16.1 s (γ = 1)
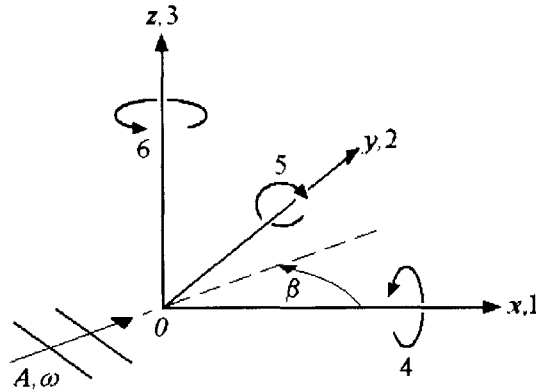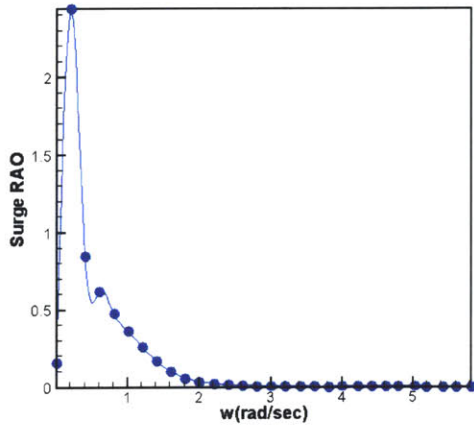

Figure 3-1: Definition of wave heading

3.3.3 *Design #1a* Performance in Environmental State 1

The RAOs for *Design #1a* in Environmental State 1 are shown below in Figure 3-2 (a) – (f). The platform's mean (static) displacement is as follows:
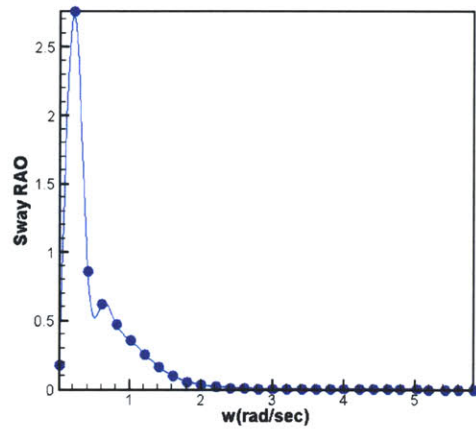
$$\xi_{1,STATIC} = 0.117 \text{ meters}$$
$$\xi_{2,STATIC} = 0.117 \text{ meters}$$
$$\xi_{3,STATIC} = 0.000 \text{ meters}$$
$$\xi_{4,STATIC} = -0.003 \text{ degrees}$$
$$\xi_{5,STATIC} = 0.003 \text{ degrees}$$
$$\xi_{6,STATIC} = 0.000 \text{ degrees}$$

and the RMS motions are

$$\sigma_1 = 1.08 \times 10^{-4} \text{ meters}$$
$$\sigma_2 = 1.09 \times 10^{-4} \text{ meters}$$
$$\sigma_3 = 1.39 \times 10^{-7} \text{ meters}$$
$$\sigma_4 = 3.00 \times 10^{-4} \text{ degrees}$$
$$\sigma_5 = 2.73 \times 10^{-4} \text{ degrees}$$
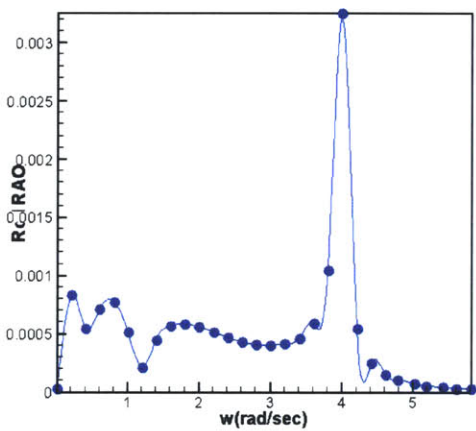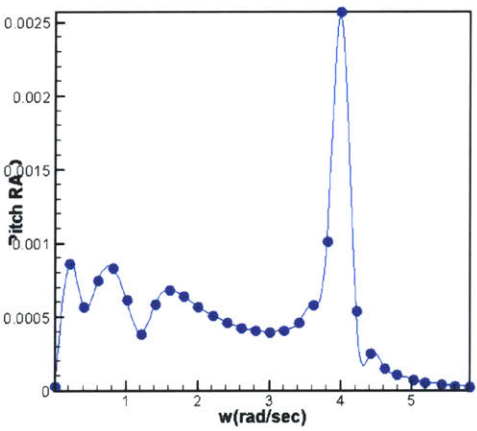$$\sigma_6 = 2.63 \times 10^{-6} \text{ degrees}$$

(a)
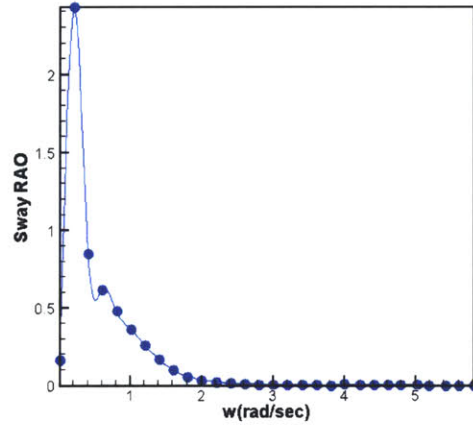
(b)
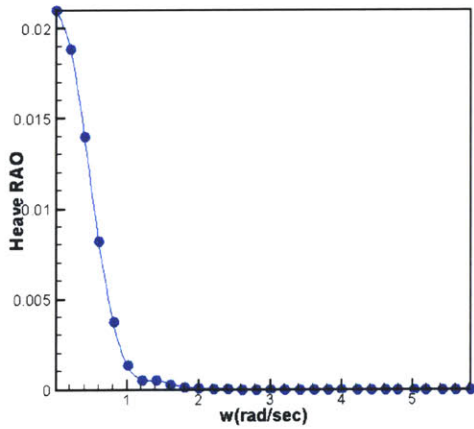
(c)
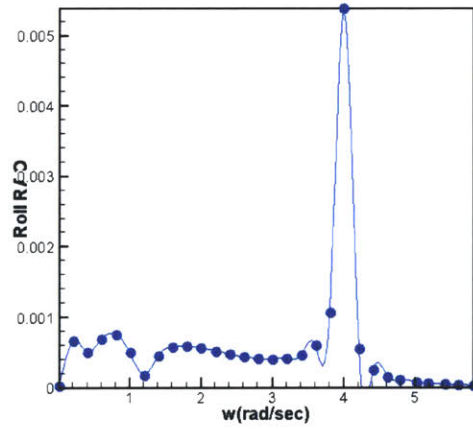
(d)
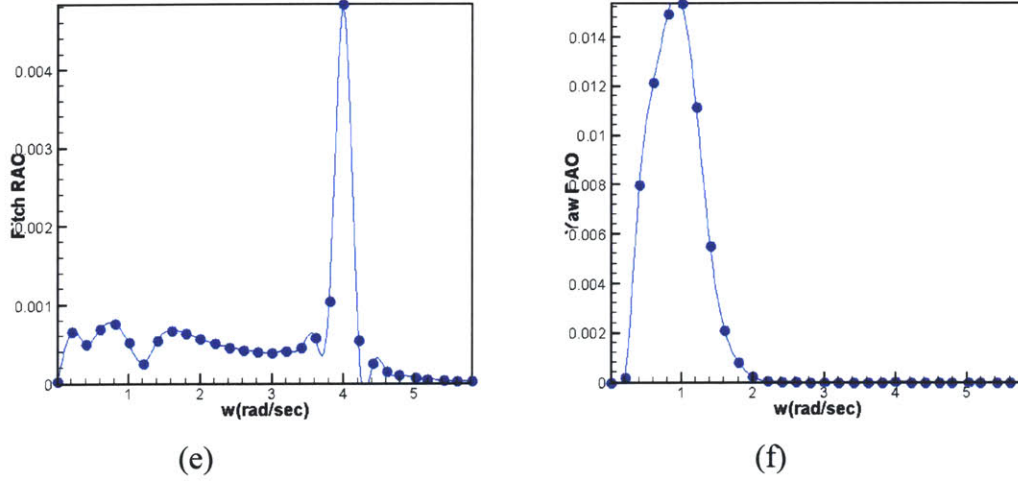
Figure 3-2 (a) – (f): RAOs for Environmental State 1

3.3.4 *Design #1a* Performance in Environmental State 2

The RAOs for *Design #1a* in Environmental State 2 are shown below in Figure 3-3 (a) –
(f). The platform's mean (static) displacement is as follows:

$$\xi_{1,STATIC} = 0.673 \text{ meters}$$
$$\xi_{2,STATIC} = 0.673 \text{ meters}$$
$$\xi_{3,STATIC} = 0.000 \text{ meters}$$
$$\xi_{4,STATIC} = -0.014 \text{ degrees}$$
$$\xi_{5,STATIC} = 0.014 \text{ degrees}$$
$$\xi_{6,STATIC} = 0.000 \text{ degrees}$$

and the RMS motions are

$$\sigma_1 = 3.00 \times 10^{-2} \text{ meters}$$
$$\sigma_2 = 3.02 \times 10^{-2} \text{ meters}$$
$$\sigma_3 = 9.04 \times 10^{-5} \text{ meters}$$
$$\sigma_4 = 8.00 \times 10^{-4} \text{ degrees}$$
$$\sigma_5 = 9.15 \times 10^{-4} \text{ degrees}$$
$$\sigma_6 = 1.18 \times 10^{-2} \text{ degrees}$$
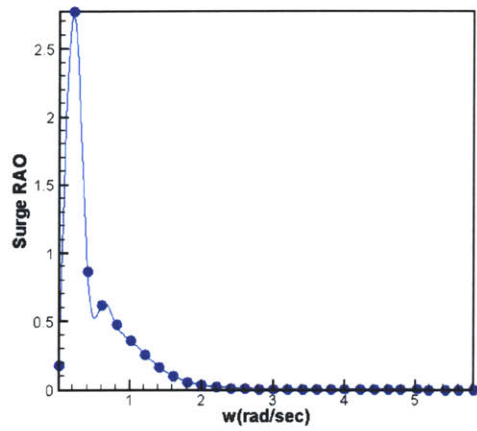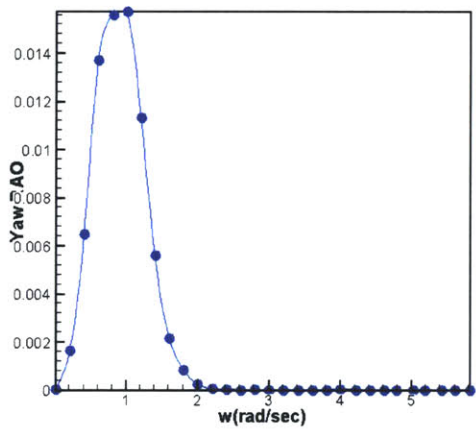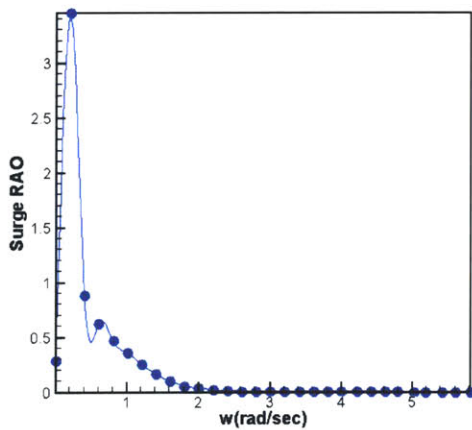
(a)

(b)
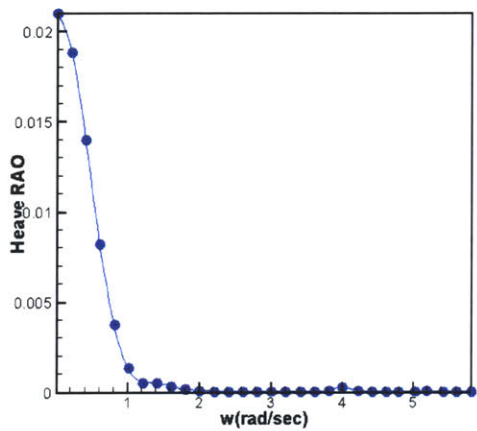
(c)

(d)

(e)

(f)

Figure 3-3 (a) – (f): RAOs for Environmental State 2

3.3.5 *Design #1a* Performance in Environmental State 3

The RAOs for *Design #1a* in Environmental State 3 are shown below in Figure 3-4 (a) – (f). The platform's mean (static) displacement is as follows:
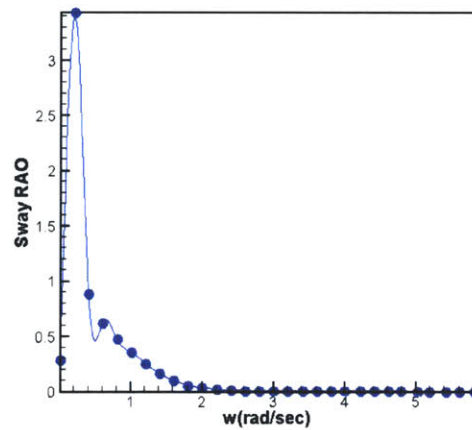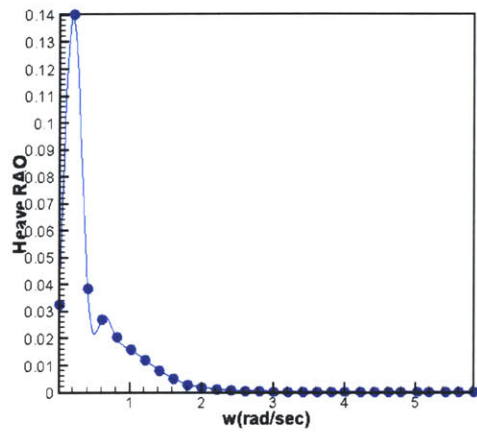
$$\xi_{1,STATIC} = 1.869 \text{ meters}$$

$$\xi_{2,STATIC} = 1.869 \text{ meters}$$

$$\xi_{3,STATIC} = 0.000 \text{ meters}$$

$$\xi_{4,STATIC} = -0.040 \text{ degrees}$$

$$\xi_{5,STATIC} = 0.040 \text{ degrees}$$

$$\xi_{6,STATIC} = 0.001 \text{ degrees}$$

and the RMS motions are

$$\sigma_1 = 0.257 \text{ meters}$$

$$\sigma_2 = 0.264 \text{ meters}$$

$$\sigma_3 = 1.15 \times 10^{-2} \text{ meters}$$

$$\sigma_4 = 5.77 \times 10^{-3} \text{ degrees}$$

$$\sigma_5 = 3.23 \times 10^{-3} \text{ degrees}$$

$$\sigma_6 = 9.87 \times 10^{-2} \text{ degrees}$$
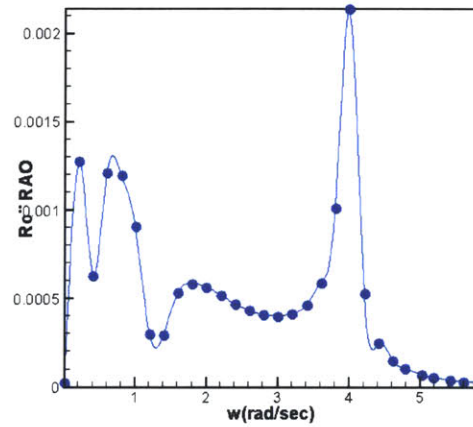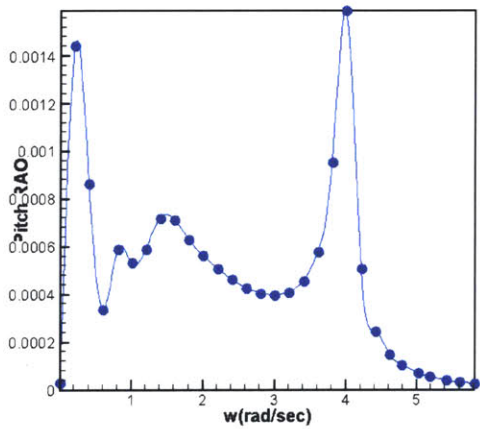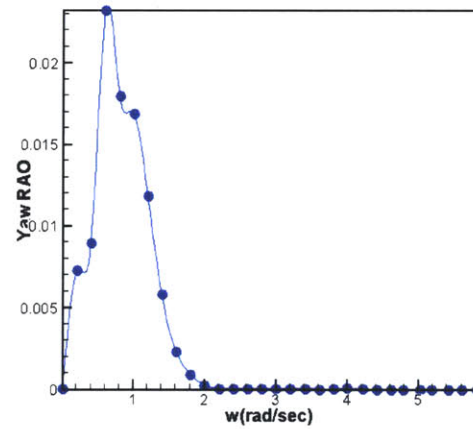

(a)

(b)

(c)

(d)

(e)

(f)

Figure 3-4 (a) – (f): RAOs for Environmental State 3

3.3.6 *Design #1a* Performance in Environmental State 4

The RAOs for *Design #1a* in Environmental State 4 are shown below in Figure 3-5 (a) – (f). The steady mean wind speed in this case, 28 knots, exceeds the *cutout speed*, or the speed above which the wind turbine can no longer operate. The wind turbine is therefore assumed to be secured, and the RMS motions of the floating system are
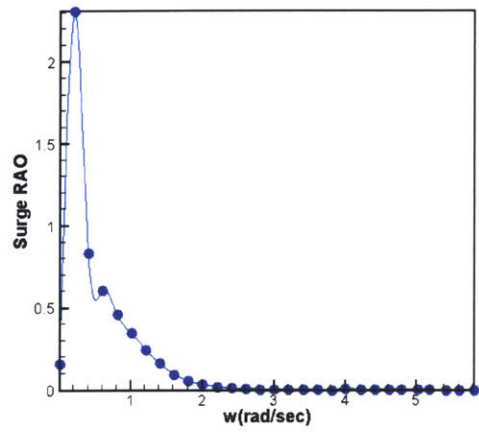
$$\sigma_1 = 0.770 \text{ meters}$$
$$\sigma_2 = 0.770 \text{ meters}$$
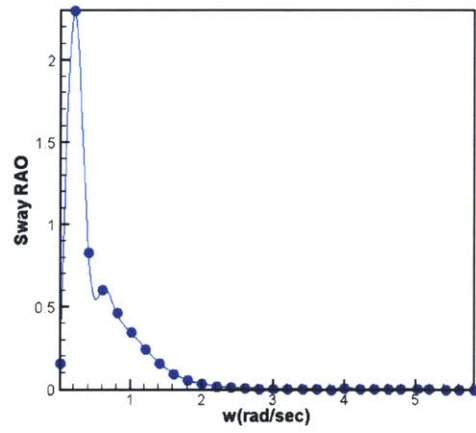$$\sigma_3 = 1.05 \times 10^{-2} \text{ meters}$$
$$\sigma_4 = 9.00 \times 10^{-3} \text{ degrees}$$
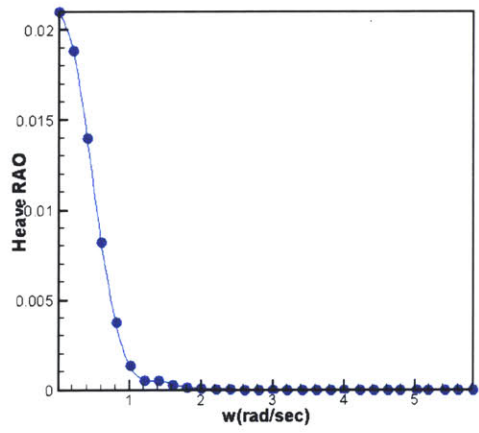$$\sigma_5 = 9.37 \times 10^{-3} \text{ degrees}$$
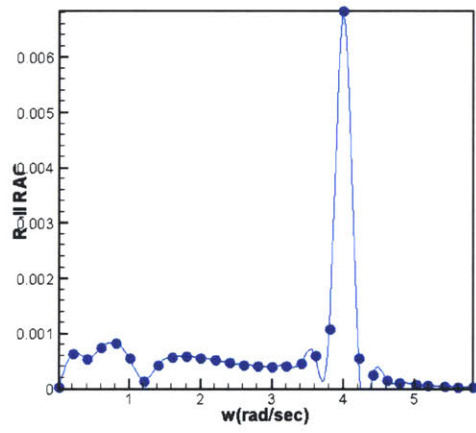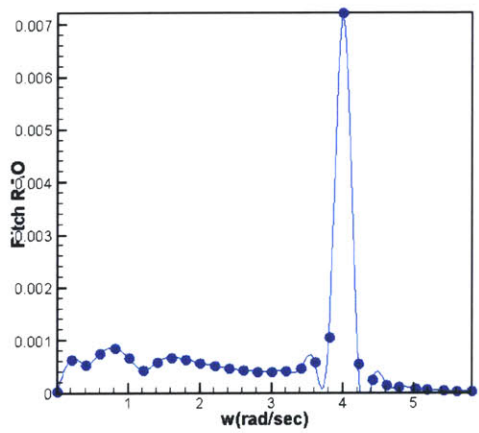$$\sigma_6 = 0.159 \text{ degrees}$$

25

Figure 3-5 (a) – (f): RAOs for Environmental State 4

3.3.7 *Design #1a* Performance in Environmental State 5

The RAOs for *Design #1a* in Environmental State 5 are shown below in Figure 3-6 (a) – (f). Again, the steady mean wind speed in this case, 40 knots, exceeds the cutout speed. The wind turbine is therefore assumed to be secured, and the RMS motions of the floating system are

$$\sigma_1 = 2.53 \text{ meters}$$
$$\sigma_2 = 2.53 \text{ meters}$$
$$\sigma_3 = 4.29 \times 10^{-2} \text{ meters}$$
$$\sigma_4 = 2.37 \times 10^{-2} \text{ degrees}$$
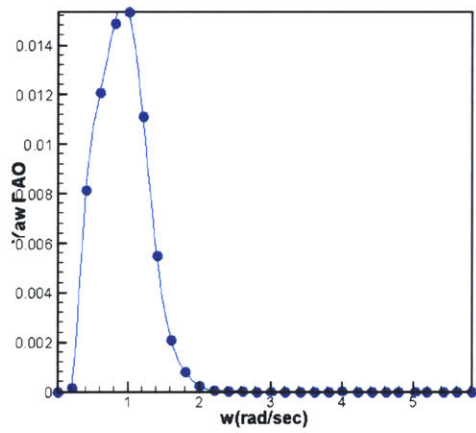$$\sigma_5 = 2.42 \times 10^{-2} \text{ degrees}$$
$$\sigma_6 = 0.328 \text{ degrees}$$
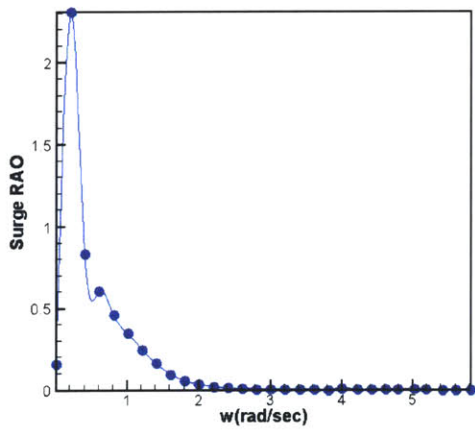

(a)

(b)

(c)

(d)

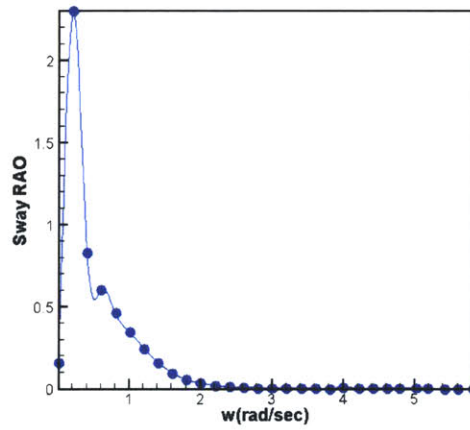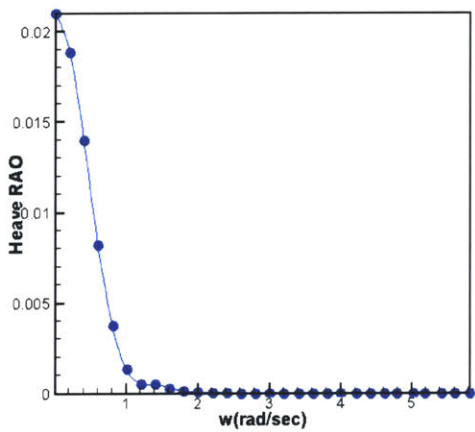Figure 3-6 (a) – (f): RAOs for Environmental State 5

3.3.8 *Design #2a* Performance in Environmental State 1

The RAOs for *Design #2a* in Environmental State 1 are shown below in Figure 3-7 (a) – (f). The platform's mean (static) displacement is as follows:

$$\xi_{1,STATIC} = 0.011 \text{ meters}$$
$$\xi_{2,STATIC} = 0.011 \text{ meters}$$
$$\xi_{3,STATIC} = 0.000 \text{ meters}$$
$$\xi_{4,STATIC} = -0.038 \text{ degrees}$$
$$\xi_{5,STATIC} = 0.038 \text{ degrees}$$
$$\xi_{6,STATIC} = 0.000 \text{ degrees}$$

and the RMS motions are

$$\sigma_1 = 1.23 \times 10^{-4} \text{ meters}$$
$$\sigma_2 = 1.23 \times 10^{-4} \text{ meters}$$
$$\sigma_3 = 3.47 \times 10^{-5} \text{ meters}$$
$$\sigma_4 = 1.11 \times 10^{-4} \text{ degrees}$$
$$\sigma_5 = 1.11 \times 10^{-4} \text{ degrees}$$
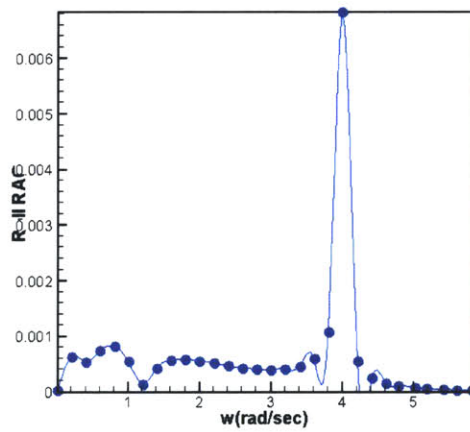$$\sigma_6 = 3.35 \times 10^{-8} \text{ degrees}$$

(a)

(b)
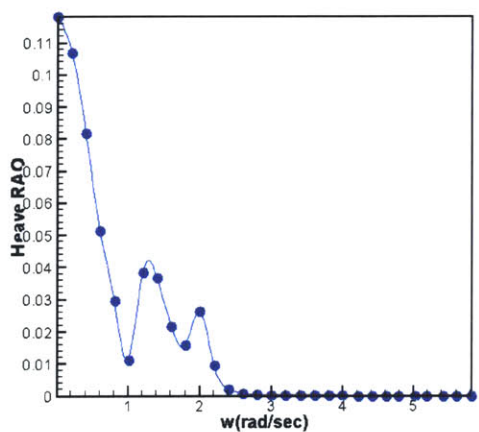
(c)

(d)

(e)

(f)

Figure 3-7 (a) – (f): RAOs for Environmental State 1

29

3.3.9 *Design #2a* **Performance in Environmental State 2**

The RAOs for *Design #2a* in Environmental State 2 are shown below in Figure 3-8 (a) – (f). The platform's mean (static) displacement is as follows:

$$\xi_{1,STATIC} = 0.062 \text{ meters}$$
$$\xi_{2,STATIC} = 0.062 \text{ meters}$$
$$\xi_{3,STATIC} = 0.000 \text{ meters}$$
$$\xi_{4,STATIC} = -0.220 \text{ degrees}$$
$$\xi_{5,STATIC} = 0.220 \text{ degrees}$$
$$\xi_{6,STATIC} = 0.000 \text{ degrees}$$

and the RMS motions are

$$\sigma_1 = 6.64 \times 10^{-2} \text{ meters}$$
$$\sigma_2 = 6.38 \times 10^{-2} \text{ meters}$$
$$\sigma_3 = 2.60 \times 10^{-2} \text{ meters}$$
$$\sigma_4 = 2.92 \times 10^{-2} \text{ degrees}$$
$$\sigma_5 = 3.28 \times 10^{-2} \text{ degrees}$$
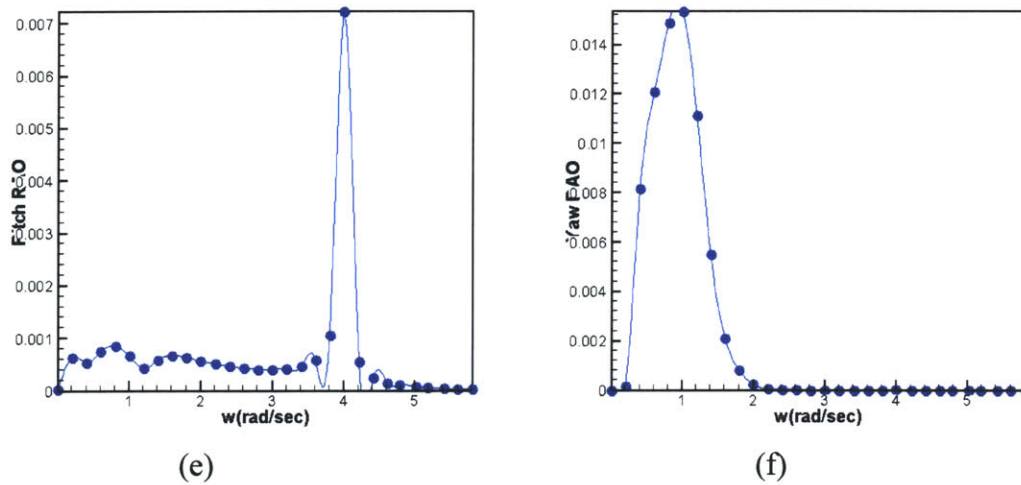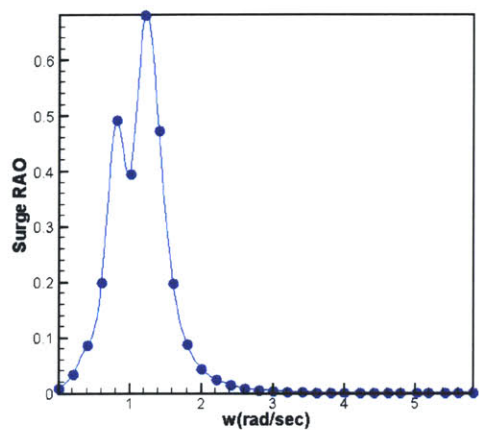$$\sigma_6 = 2.99 \times 10^{-2} \text{ degrees}$$
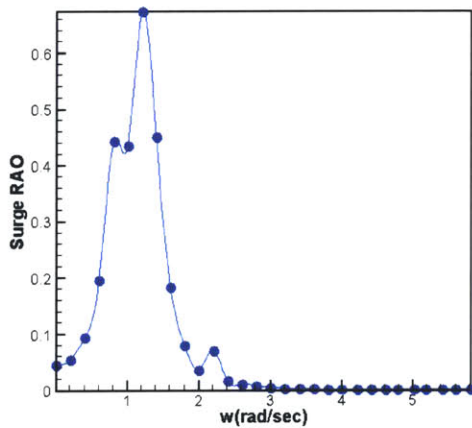
(a)
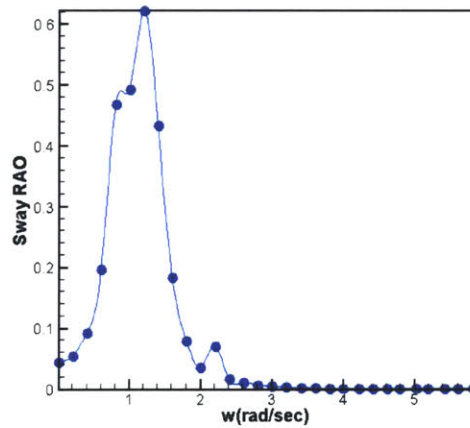
(b)

Figure 3-8 (a) – (f): RAOs for Environmental State 1

3.3.10 *Design #2a* Performance in Environmental State 3

The RAOs for *Design #2a* in Environmental State 3 are shown below in Figure 3-9 (a) – (f). The platform's mean (static) displacement is as follows:
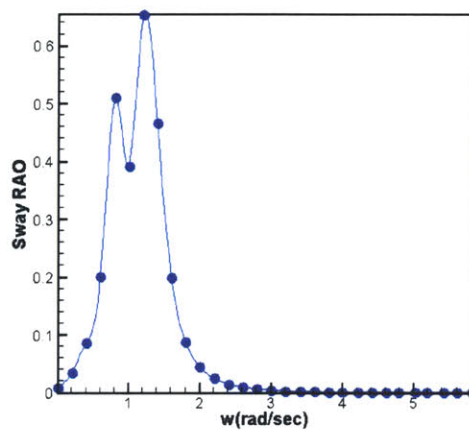
$$\xi_{1,STATIC} = 0.173 \text{ meters}$$
$$\xi_{2,STATIC} = 0.173 \text{ meters}$$
$$\xi_{3,STATIC} = 0.000 \text{ meters}$$
$$\xi_{4,STATIC} = -0.612 \text{ degrees}$$
$$\xi_{5,STATIC} = 0.612 \text{ degrees}$$
$$\xi_{6,STATIC} = 0.000 \text{ degrees}$$

31

and the RMS motions are

$$\sigma_1 = 0.253 \text{ meters}$$
$$\sigma_2 = 0.270 \text{ meters}$$
$$\sigma_3 = 0.158 \text{ meters}$$
$$\sigma_4 = 0.102 \text{ degrees}$$
$$\sigma_5 = 0.213 \text{ degrees}$$
$$\sigma_6 = 0.475 \text{ degrees}$$
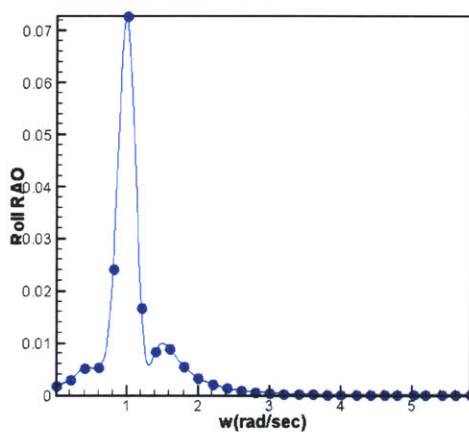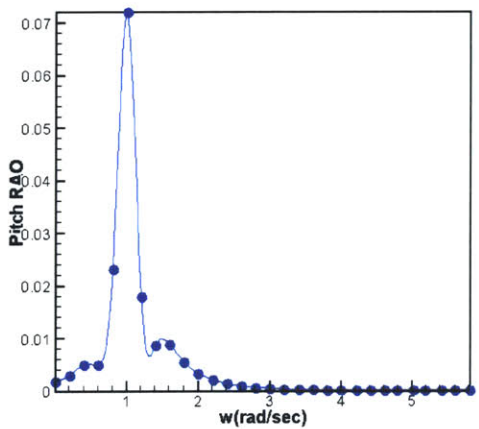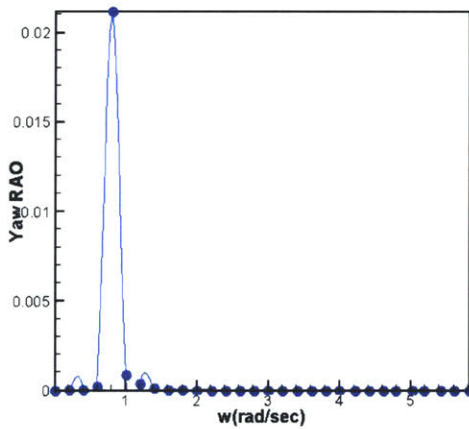

(a)

(b)

(c)

(d)

32
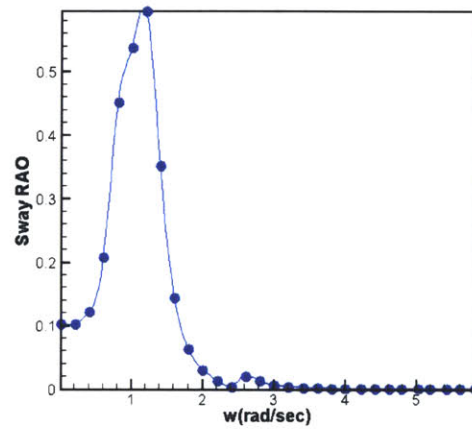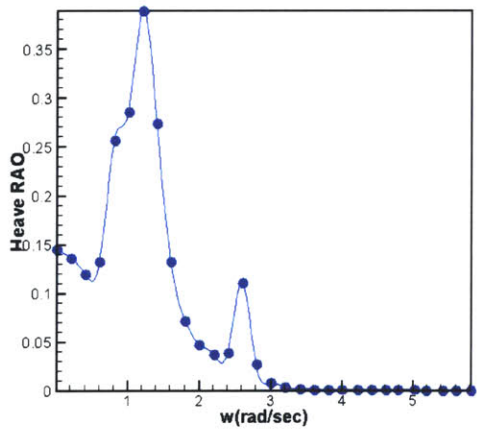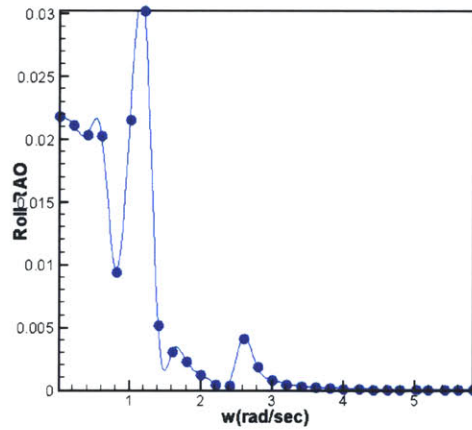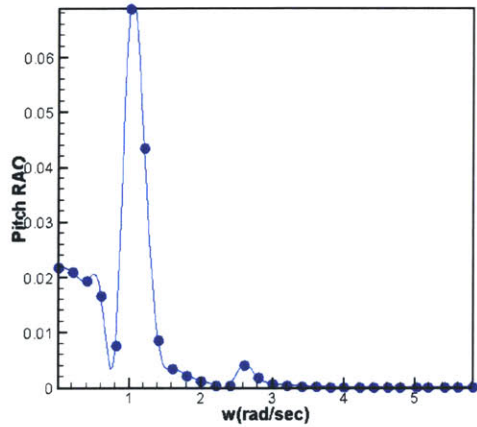
(e)
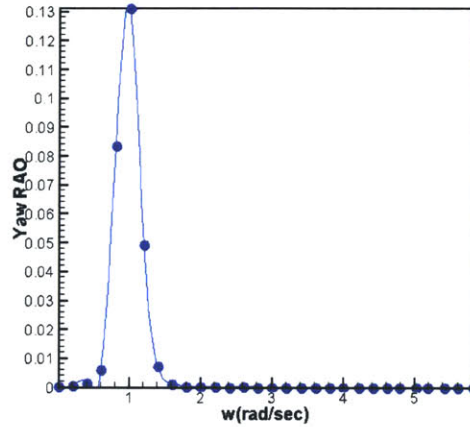
(f)

Figure 3-9 (a) – (f): RAOs for Environmental State 1

3.3.11 *Design #2a* **Performance in Environmental State 4**

The RAOs for *Design #2a* in Environmental State 4 are shown below in Figure 3-10 (a) – (f). The steady mean wind speed in this case, 28 knots, exceeds the *cutout speed*, or the speed above which the wind turbine can no longer operate. The wind turbine is therefore assumed to be secured, and the RMS motions of the floating system are

$$\sigma_1 = 0.402 \text{ meters}$$
$$\sigma_2 = 0.402 \text{ meters}$$
$$\sigma_3 = 6.42 \times 10^{-2} \text{ meters}$$
$$\sigma_4 = 0.381 \text{ degrees}$$
$$\sigma_5 = 0.381 \text{ degrees}$$
$$\sigma_6 = 0.000 \text{ degrees}$$

(a)   (b)

(c)   (d)

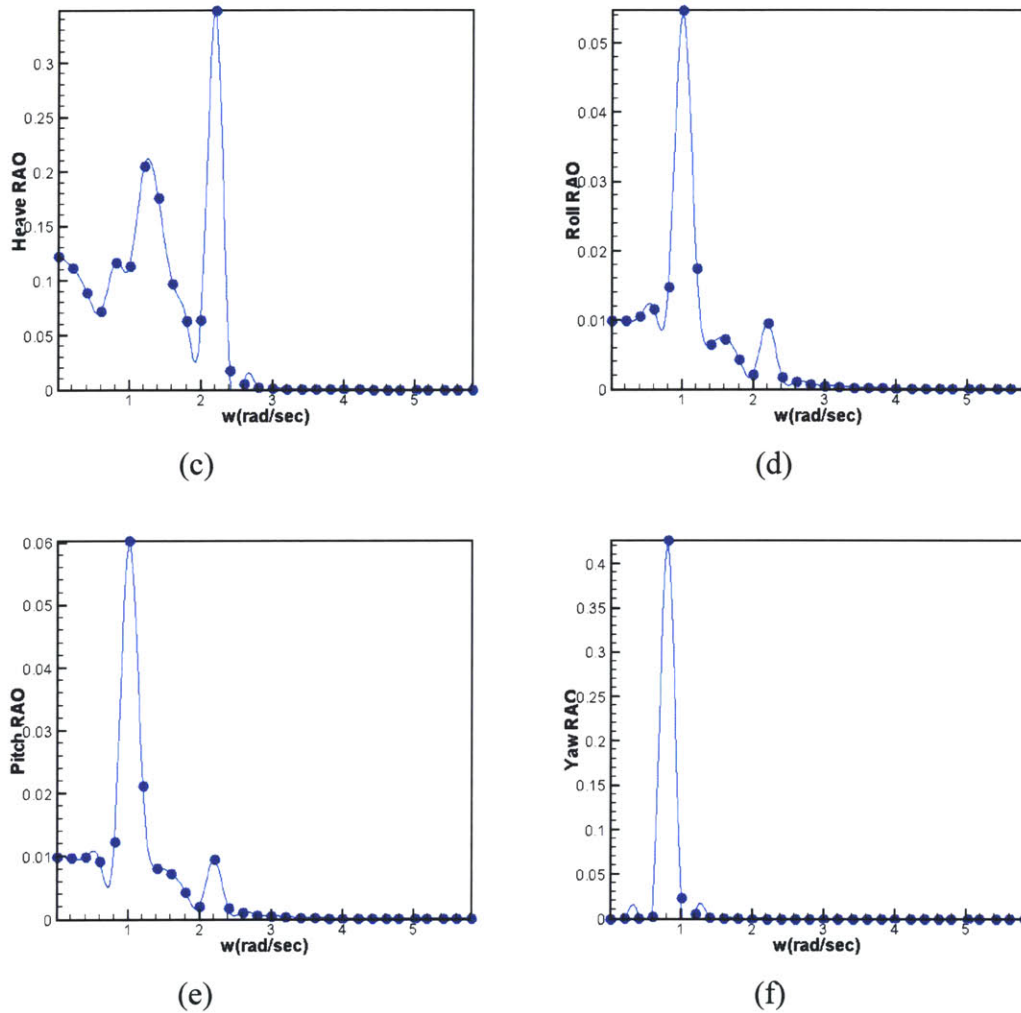(e)   (f)
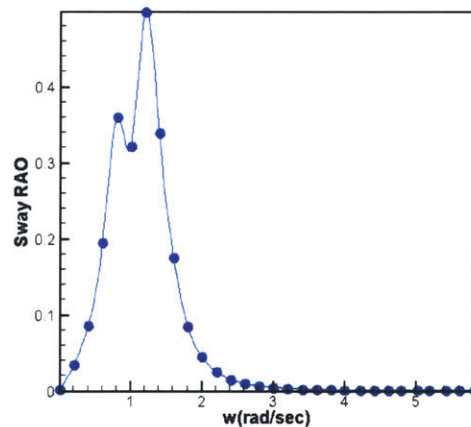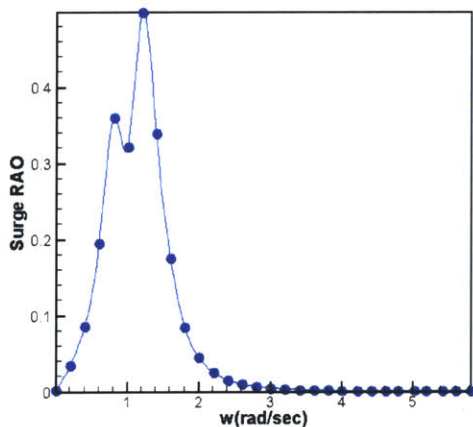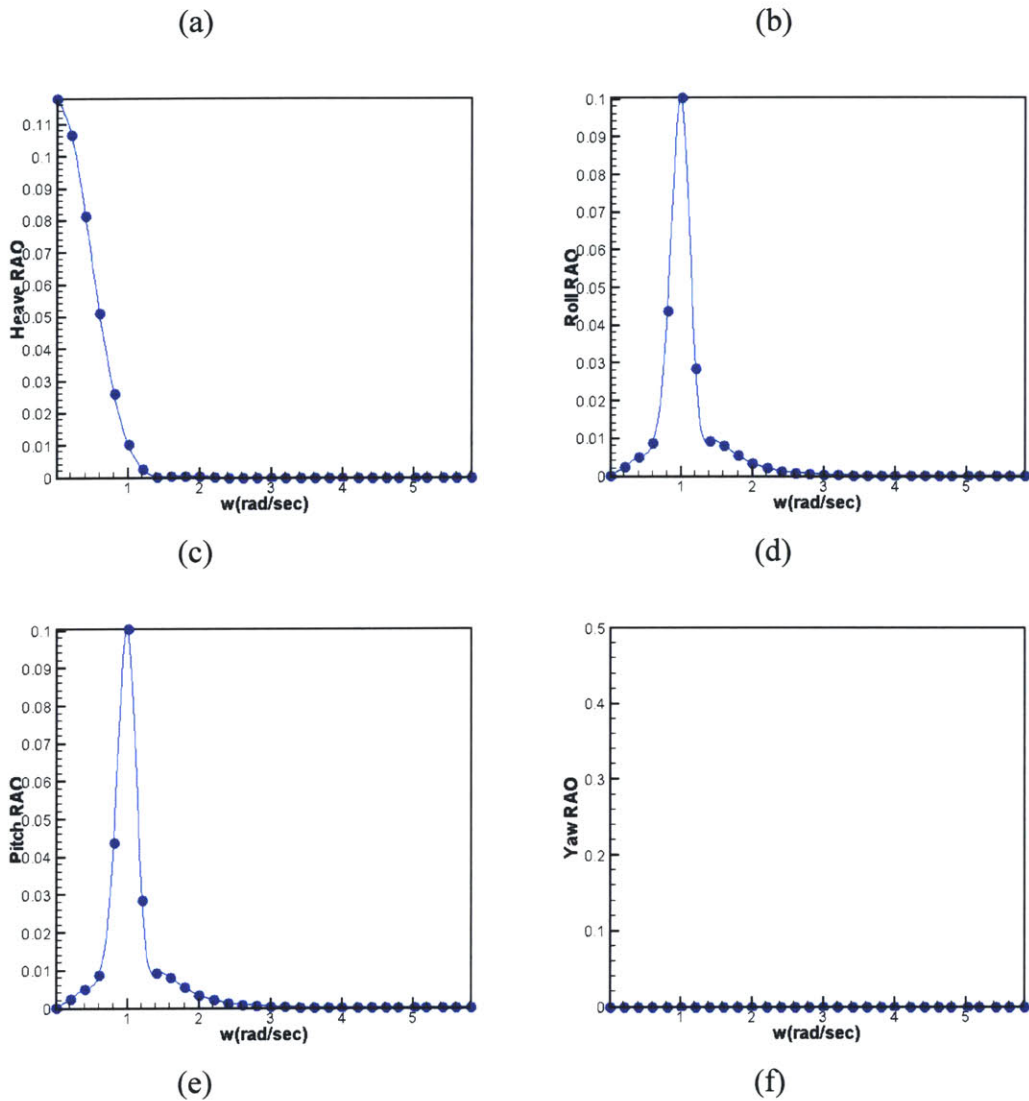
Figure 3-10 (a) – (f): RAOs for Environmental State 4

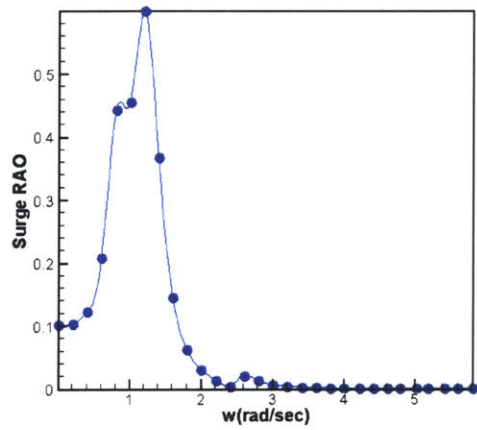### 3.3.12 *Design #2a* **Performance in Environmental State 5**

The RAOs for *Design #2a* in Environmental State 5 are shown below in Figure 3-11 (a) – (f). The steady mean wind speed in this case, 28 knots, exceeds the *cutout speed*, or the speed above which the wind turbine can no longer operate. The wind turbine is therefore assumed to be secured, and the RMS motions of the floating system are

$$\sigma_1 = 0.562 \text{ meters}$$
$$\sigma_2 = 0.562 \text{ meters}$$
$$\sigma_3 = 0.252 \text{ meters}$$
$$\sigma_4 = 0.637 \text{ degrees}$$
$$\sigma_5 = 0.637 \text{ degrees}$$
$$\sigma_6 = 0.000 \text{ degrees}$$
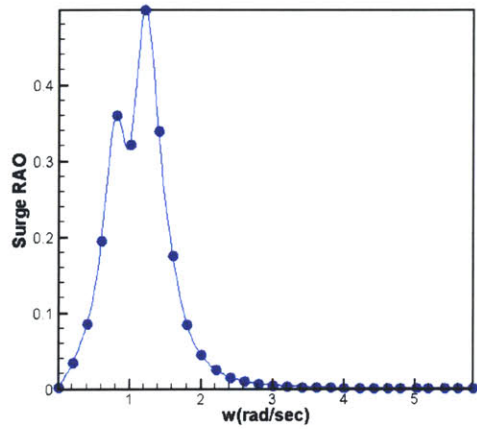
(a)
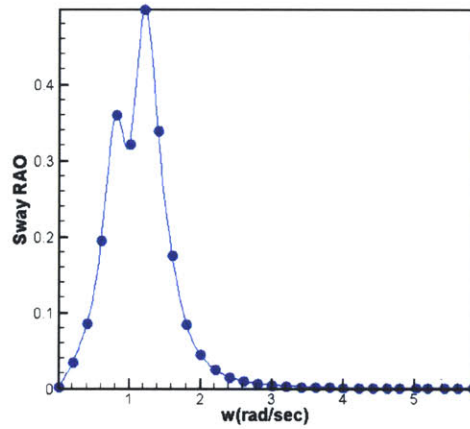
(b)
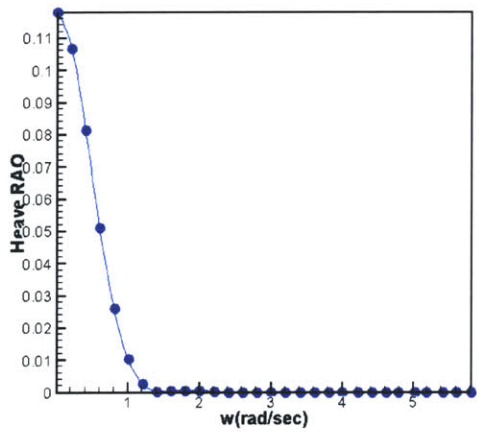
(c)
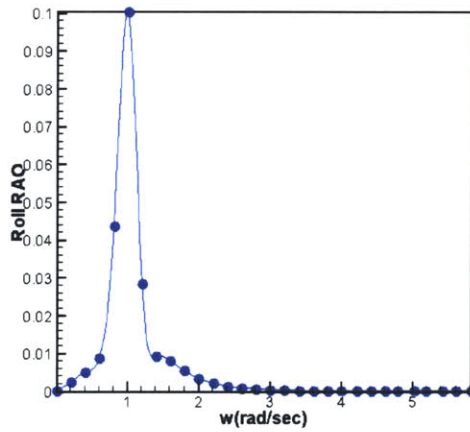
(d)
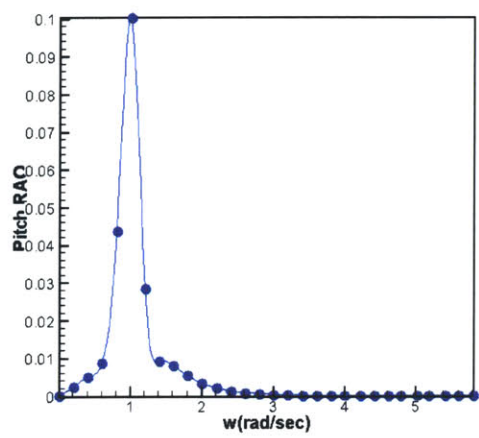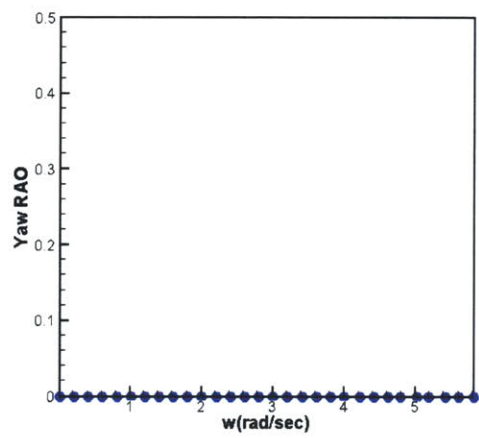
(e)   (f)

Figure 3-11 (a) – (f): RAOs for Environmental State 5

Chapter 4

Nonlinear Wave Excitation

4.1 Introduction

The second part of this thesis will examine a new approach to computing the nonlinear wave excitation upon a truncated vertical circular cylinder. This approach may be used to compute the nonlinear wave loads upon slender cylindrical structures such as floating wind turbines and other offshore structures. The results show some interesting nonlinear phenomena that have been observed in previous experimental research.

4.2 Long Wavelength Approximation

A long wavelength approximation can be used to predict the wave excitation for cases where the characteristic dimension of the structure (such as the diameter) is much less than the wavelength of the ambient waves.

The accurate prediction of nonlinear wave loads depends critically on the precise modeling of the unsteady particle accelerations in the fluid. Using a fundamental relation derived in a recent study by Sclavounos (2003), the particle kinematics on the exact position of the free surface is computed, and it is used to estimate the particle accelerations in the fluid domain by interpolation. This approach is seen to be more accurate than the often-used procedure of extrapolating the particle kinematics from their values near the mean position of the free surface using linear theory.

4.3 Wave Excitation of a Truncated Vertical Cylinder

The surge exciting force on a vertical circular cylinder in plane progressive waves of length $\lambda \gg d$ (the diameter of the cylinder) advancing in the $+x$-direction may be expressed as

$$dX_1 = 2\rho\pi r^2 \left(\frac{\partial u}{\partial t} + u\frac{\partial u}{\partial x} + w\frac{\partial u}{\partial z} \right)_{x=x_0,z} dz \qquad (4.1)$$

where u is the fluid velocity in the x-direction, w is the fluid velocity in the z-direction, and $x = x_0$ is the location of the cylinder.

The nonlinear acceleration term can be estimated by interpolating from the particle acceleration on the exact free surface by an exponential decay law using the wavenumber, k, corresponding to the carrier wave. Thus (4.1) may be rewritten as follows:

$$dX_1 = 2\rho\pi r^2 \ddot{\eta}_{1,x=x_0}(t)e^{k(z-\zeta)}dz \tag{4.2}$$

where $\zeta(x,t)$ is the wave elevation and $\ddot{\eta}_{1,x=x_0}(t)$ is the horizontal particle acceleration of the particle at $x = x_0$ at time t.

The surge exciting force on a truncated cylinder of draft T is then

$$X_1(t) = \int_{-T}^{\zeta(t)} dX_1 \tag{4.3}$$

while the pitch exciting moment is

$$X_5(t) = \int_{-T}^{\zeta(t)} z \, dX_1 \tag{4.4}$$

The hydrostatic contribution is the leading order effect in the heave exciting force, which may be expressed as

$$X_3(t) = \rho g A_{WP} \zeta(x_0,t) \tag{4.5}$$

where A_{WP} is the waterplane area of the cylinder.

4.4   Wave Particle Kinematics

4.4.1   Particle Evolution Equation

The horizontal particle acceleration term in (4.2) is computed by solving the free-surface particle evolution equation derived by Sclavounos. Figure 4-1 shows a plane progressive wave and the instantaneous vector position of a fluid particle on the free surface.
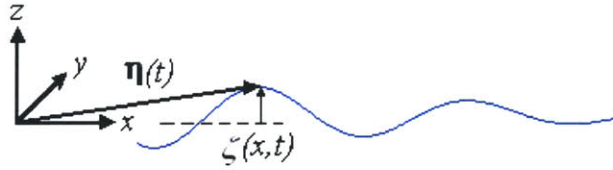
Figure 4-1: Definition of the free surface elevation $z = \zeta(x,t)$ and the instantaneous vector position of a fluid particle on the free surface $\boldsymbol{\eta}(t) = (\eta_1(t),\eta_3(t))$

The two-dimensional particle evolution equation is then as follows:

$$\frac{d^2\eta_1}{dt^2} + P(\eta_1,t)\frac{d\eta_1}{dt} + Q(\eta_1,t)\left(\frac{d\eta_1}{dt}\right)^2 = R(\eta_1,t) \tag{4.6}$$

38

where

$$P(\eta_1,t) = \cfrac{2\,\cfrac{\partial \zeta(x=\eta_1,t)}{\partial x}\,\cfrac{\partial^2 \zeta(x=\eta_1,t)}{\partial x \partial t}}{1 + \left(\cfrac{\partial \zeta(x=\eta_1,t)}{\partial x}\right)^2}$$

(4.7)

$$Q(\eta_1,t) = \cfrac{\cfrac{\partial \zeta(x=\eta_1,t)}{\partial x}\,\cfrac{\partial^2 \zeta(x=\eta_1,t)}{\partial x^2}}{1 + \left(\cfrac{\partial \zeta(x=\eta_1,t)}{\partial x}\right)^2}$$

(4.8)

$$R(\eta_1,t) = \cfrac{-\cfrac{\partial \zeta(x=\eta_1,t)}{\partial x}\left(\cfrac{\partial^2 \zeta(x=\eta_1,t)}{\partial t^2} + g\right)}{1 + \left(\cfrac{\partial \zeta(x=\eta_1,t)}{\partial x}\right)^2}$$

(4.9)

4.4.2 Description of Waves

Two types of ambient waves are examined for the validation of the numerical solution of (4.6): regular plane progressive waves and Stokes 2nd-order waves in deep water. The free surface elevation for regular plane progressive waves propagating into calm water is defined as

$$\zeta(x,t) = \frac{1}{2}\left[1 - \tanh\left(\frac{kx - a_1\omega t}{a_2}\right)\right][A\cos(kx - \omega t)]$$

(4.10)

For Stokes 2nd-order waves propagating into calm water, the free surface elevation is given as

$$\zeta(x,t) = \frac{1}{2}\left[1 - \tanh\left(\frac{kx - a_1\omega t}{a_2}\right)\right][A\cos(kx - \omega t) + \tfrac{1}{2}kA^2 \cos 2(kx - \omega t)]$$

(4.11)

A and ω represent the wave amplitude and frequency, respectively. The parameter a_1 determines the speed of the wave front (the front travels at phase velocity for $a_1 = 1$, and at group velocity for $a_1 = \frac{1}{2}$). The non-dimensional parameter, kA/a_2, governs the steepness of the wave front. For waves of small steepness ($kA \ll 1$), values of $kA/a_2 \leq$ 0.005 mitigate the solution's sensitivity to the speed of the wave front. For waves of finite steepness, this value becomes $kA/a_2 \leq 0.002$.

4.4.3 Solution of the Particle Evolution Equation and Validation

The numerical solution of (4.6-9) was carried out for a fluid particle on the free surface with an initial position well ahead of the wave front such that $\dot{\eta}_1(t=0)=0$. In fact, the purpose of creating an artificial wave front was so that the exact value of the Eulerian horizontal velocity at the location of the particle would be known (in order to specify the appropriate initial conditions).

For the validation of the solution, the resulting mean horizontal drift velocity of the particle was compared with the so-called *Stokes' drift velocity*, given as

$$U_{Stokes} = \omega k A^2 \tag{4.12}$$

for waves of small steepness.

4.4.3.1 Regular plane progressive waves

For regular plane progressive waves of $A = 1$ m, $\omega = 0.5$ rad/s, and $a_2 = 6$ ($kA/a_2 = 0.0042$), the horizontal particle trajectory is as shown in Figure 4-2 (a) and (b) – corresponding to values of $a_1 = 1$ and $a_1 = \frac{1}{2}$.

(a): $a_1 = 1$ (b): $a_1 = \frac{1}{2}$
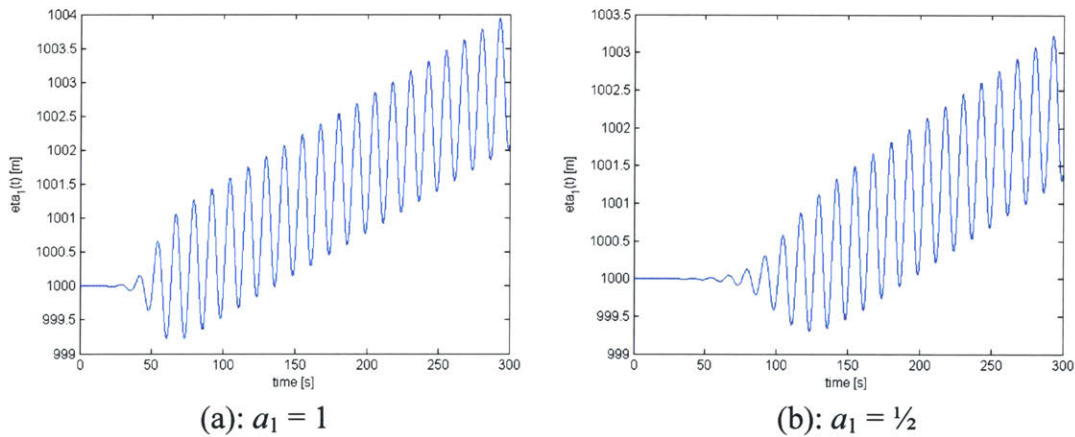
Figure 4-2 (a) – (b): Horizontal trajectory of a particle with initial position $x = 1,000$ m

For the case where $a_1 = 1$, the steady mean drift velocity is 0.0128 m/s, while for the case where $a_1 = \frac{1}{2}$, the steady mean drift velocity is 0.0127 m/s. It is observed that once a steady state has been reached, the solution is independent of the speed of the wave front. Furthermore, good agreement is shown with the Stokes' drift velocity $U_{Stokes} = 0.0127$ m/s.

4.4.3.2 Stokes 2nd-order waves

For Stokes 2nd-order waves of $A = 1$ m, $\omega = 0.5$ rad/s, and $a_2 = 6$ ($kA/a_2 = 0.0042$), the horizontal particle trajectory is as shown in Figure 4-3 (a) and (b) – corresponding to values of $a_1 = 1$ and $a_1 = \frac{1}{2}$.

(a): $a_1 = 1$ (b): $a_1 = \frac{1}{2}$
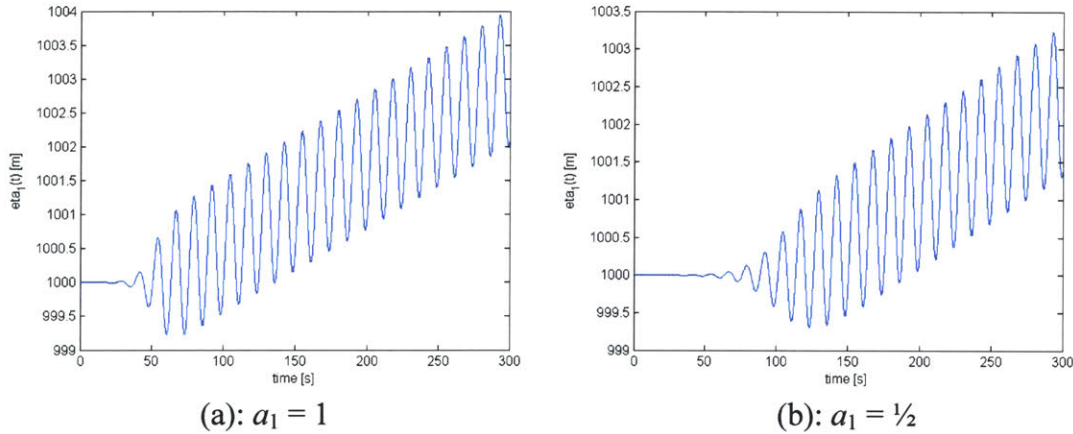
Figure 4-3 (a) – (b): Horizontal trajectory of a particle with initial position $x = 1,000$ m

For the case where $a_1 = 1$, the steady mean drift velocity is 0.0126 m/s, while for the case where $a_1 = \frac{1}{2}$, the steady mean drift velocity is 0.0125 m/s. Again, it is observed that once a steady state has been reached, the solution is independent of the speed of the wave front. Furthermore, good agreement is shown with the Stokes' drift velocity $U_{Stokes} = 0.0127$ m/s.

4.5 Excitation Due to Regular Plane Progressive Waves of Finite Steepness

For the present study, the excitation of a truncated vertical circular cylinder by regular plane progressive waves of frequency $\omega = 0.4$ rad/s and amplitude $A = 9.8$ m ($kA = 0.16$) is examined. The surge and pitch excitation will be computed according to (4.2-4) where the nonlinear kinematics are computed by solving the particle evolution equations. The ambient wave elevation at the location of the cylinder is shown in Figure 4-4.

41
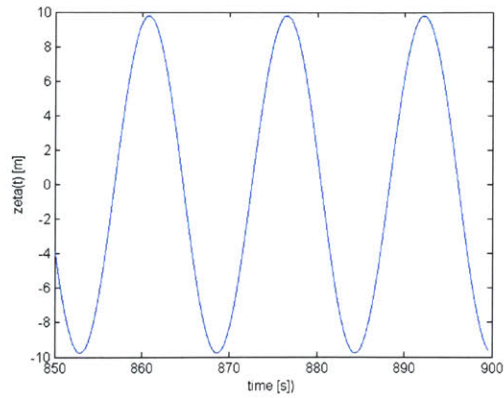
Figure 4-4: Periodic regular waves of frequency $\omega = 0.4$ rad/s and amplitude $A = 9.8$ m

4.5.1 Results: Excitation of Higher Harmonics

The wave excitation of a truncated vertical cylinder of draft $T = 15$ m and radius $r = 6$ m is shown in Figure 4-5 (a) – (b).
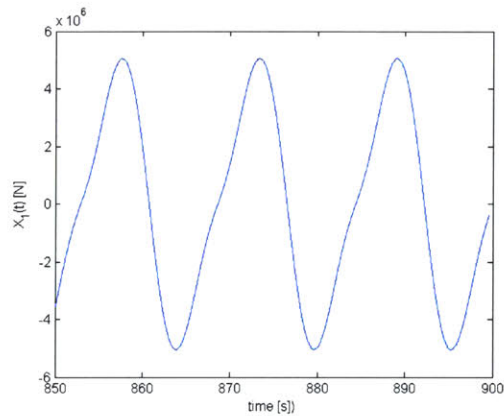
(a): Surge
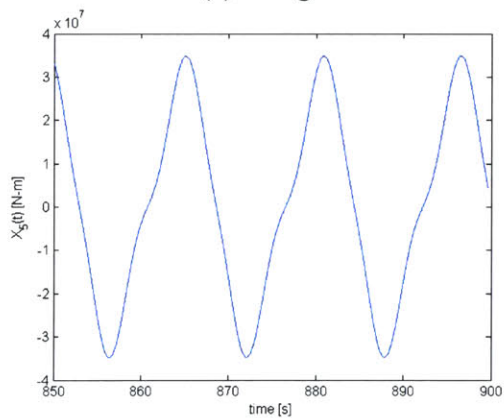
(b): Pitch

Figure 4-5 (a) – (b): Excitation

As observed in an experimental study by Grue and Huseby (2002), a secondary load cycle appears in the surge and pitch excition. For purposes of design, it may be important to consider the excitation of higher harmonics – in particular, to avoid resonance with the turbine rotor or the above-waterline structure. This may be a topic of further study.

The surge and pitch responses of *Design #1a* and *Design #2a* to the excitation computed above are shown below in Figures 4-6 and 4-7, respectively (the details of the time-domain calculation are described in Appendix C).
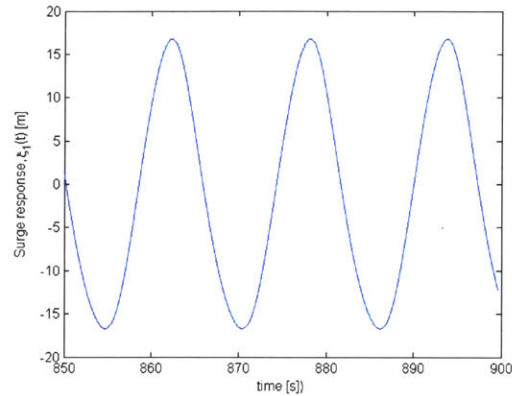
(a): Surge
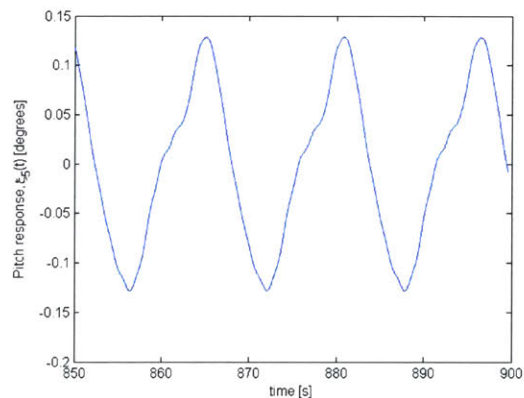
(b): Pitch

Figure 4-6 (a) – (b): Responses of *Design #1a*
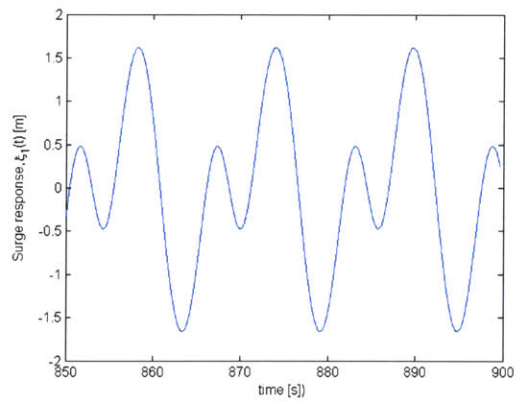
(a): Surge
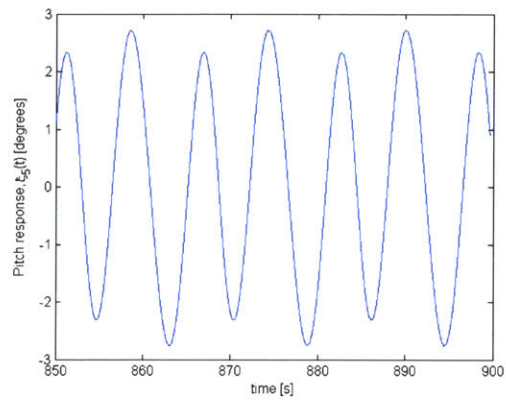
(b): Pitch

Figure 4-7 (a) – (b): Responses of *Design #2a*

Chapter 5

Discussion and Conclusions

Two concept designs for floating wind turbine systems were proposed in this study: a tension-leg platform (*Design #1a*) and a taut-leg moored system (*Design #2a*). The analysis shows *Design #1a* to be relatively soft in surge and sway but extremely stiff in the rotational modes. In contrast, *Design #2a* is shown to be stiff in surge and sway but softer than *Design #1a* in the rotational modes. Furthermore, the natural frequencies of *Design #1a* tend to be in the very low frequency region (0.2 ~ 0.3 rad/s) or high frequency region (~ 4 rad/s), for which there is little energy in typical ocean spectra. The natural frequencies of *Design #2a* are in the region for which there is significant energy in typical ocean spectra; nevertheless, the RMS roll and pitch response does not exceed one degree even in the severest sea state. A summary of the performances of both concept designs is given in Table 5-1.

Design #1a	Env. State 1	Env. State 2	Env. State 3	Env. State 4	Env. State 5
σ_1 (m)	1.08E-04	3.00E-02	0.257	0.770	2.53
σ_2 (m)	1.09E-04	3.02E-02	0.264	0.770	2.53
σ_3 (m)	1.39E-07	9.04E-05	1.15E-02	1.05E-02	4.29E-02
σ_4 (deg)	3.00E-04	8.00E-04	5.77E-03	9.00E-03	2.37E-02
σ_5 (deg)	2.73E-04	9.15E-04	3.23E-03	9.37E-03	2.42E-02
σ_6 (deg)	2.63E-06	1.18E-02	9.87E-02	0.159	0.328

Design #2a	Env. State 1	Env. State 2	Env. State 3	Env. State 4	Env. State 5
σ_1 (m)	1.23E-04	6.64E-02	0.253	0.402	0.562
σ_2 (m)	1.23E-04	6.38E-02	0.270	0.402	0.562
σ_3 (m)	3.47E-05	2.60E-02	0.158	6.42E-02	0.252
σ_4 (deg)	1.11E-04	2.92E-02	0.102	0.381	0.637
σ_5 (deg)	1.11E-04	3.28E-02	0.213	0.381	0.637
σ_6 (deg)	3.35E-08	2.99E-02	0.475	0.000	0.000

Table 5-1: Summary of performance

In general, a three-legged mooring system would be preferred from the view of reducing foundation costs. However, a three-legged mooring configuration of the type of *Design #2a* has been found to have a strongly negative value for $C_{64,LINES}$, resulting in the excitation of large amplitude yaw motions. The addition of a fourth leg completely decouples yaw from the other modes of motion. This problem does not seem to exist in the case of the tension-leg platform design.

Finally, a new approach to computing the nonlinear wave excitation was presented. The computational results show the excitation of higher harmonics as observed in previous experimental research. For purposes of design, it may be important to consider these higher harmonics, particularly to avoid resonance with the turbine rotor or the above-waterline structure. As a topic of further research, the floating wind turbine system's response to extreme wave events (wave focusing or steep, near-breaking waves) may be investigated.

Again, it is emphasized that the analysis contained in this thesis is preliminary. The entire floating wind turbine system has been modeled as a rigid body and only the case of steady wind loading has been considered. Possible future research might include the case of unsteady wind loading and an evaluation of performance in stochastic waves in the time-domain.

Appendix A

Stability Criteria

A.1 Statement of the Eigenvalue Problem

The equations of motion for the floating wind turbine in free vibration are

$$(\mathbf{M} + \mathbf{A})\ddot{\xi} + \mathbf{B}\dot{\xi} + \mathbf{C}\xi = 0 \tag{1}$$

where $\mathbf{M}$ is the mass matrix, $\mathbf{A}$ is the zero-frequency added mass matrix, $\mathbf{B}$ is the damping matrix, $\mathbf{C}$ is the restoring matrix, and ξ is the floating wind turbine response where $\xi \in \mathbb{R}^6$ and $\mathbf{M}$, $\mathbf{A}$, $\mathbf{B}$, and $\mathbf{C}$ are 6×6 matrices.

Setting $\mathbf{y}_1 = \xi$ and $\mathbf{y}_2 = \dot{\mathbf{y}}_1$, (1) may be rewritten as follows:

$$\begin{pmatrix} \mathbf{I} & 0 \\ 0 & \mathbf{M} + \mathbf{A} \end{pmatrix} \begin{pmatrix} \dot{\mathbf{y}}_1 \\ \dot{\mathbf{y}}_2 \end{pmatrix} = \begin{pmatrix} 0 & \mathbf{I} \\ -\mathbf{C} & -\mathbf{B} \end{pmatrix} \begin{pmatrix} \mathbf{y}_1 \\ \mathbf{y}_2 \end{pmatrix} \tag{2}$$

Now let

$$\mathbf{x} = \begin{pmatrix} \mathbf{y}_1 \\ \mathbf{y}_2 \end{pmatrix} \tag{3}$$

and

$$A = \begin{pmatrix} \mathbf{I} & 0 \\ 0 & \mathbf{M} + \mathbf{A} \end{pmatrix}^{-1} \begin{pmatrix} 0 & \mathbf{I} \\ -\mathbf{C} & -\mathbf{B} \end{pmatrix} \tag{4}$$

where A is a 12×12 matrix. Then (1) can be written

$$\dot{\mathbf{x}} = A\mathbf{x} \tag{5}$$

The solution of the linear system (5) together with the initial condition $\mathbf{x}(0) = \mathbf{x}_0$ is given by

$$\mathbf{x}(t) = c_1 e^{\lambda_1 t} \mathbf{x}_1 + c_2 e^{\lambda_2 t} \mathbf{x}_2 + \ldots + c_{12} e^{\lambda_{12} t} \mathbf{x}_{12} \tag{6}$$

where λ_i are the complex eigenvalues of the matrix A and $\mathbf{x}_i$ are the eigenmodes.

A.2 Stability Criteria

The stability criteria for the system is as described in a standard text in dynamics (Williams 1996):

1. If at least one of the real parts of the eigenvalues is positive, then the equilibrium state of the system is *unstable*.
2. If all of the real parts of the eigenvalues are negative, then the equilibrium state of the system is *asymptotically stable*.
3. If at least one of the real parts of the eigenvalues is zero and all the rest of the real parts of the roots are negative, then the equilibrium state of the linearized system is *marginally stable*.

Appendix B

Calculation of Aerodynamic Loading and Damping Coefficients

This section develops expressions for the aerodynamic loading $X_{1,AERO}$ and the damping coefficients $B_{ij,AERO}$.

The aerodynamic force, or *thrust*, upon a wind turbine fixed in space is $T_0 = T_0(U)$, where T_0 is a nonlinear function of the ambient wind velocity U. If the wind turbine is allowed to oscillate about its mean position, this thrust becomes $T_0 = T_0(U - \dot{x})$, where $\dot{x}$ is the velocity of the structure at the center of the rotor disc ($z = z_d$).

Assuming that $|\dot{x}| \ll U$, we can expand this expression as follows:

$$T_0(U - \dot{x}) = T_0(U) - \dot{x}\frac{\partial T_0(U)}{\partial U} + O(\dot{x}^2) \tag{1}$$

Neglecting the higher-order terms, and noting that for motions restricted to the xz-plane, $\dot{x} = \dot{\xi}_1 + z_d\dot{\xi}_5$, the total thrust upon the wind turbine may be written:

$$T_0(U, \dot{\xi}_1, \dot{\xi}_5) = T_0(U) - \frac{\partial T_0(U)}{\partial U}(\dot{\xi}_1 + z_d\dot{\xi}_5) \tag{2}$$

The aerodynamic surge loading on the floating wind turbine is then

$$X_{1,AERO} = T_0(U) \tag{3}$$

while the damping coefficients are

$$B_{11,AERO} = \frac{\partial T_0(U)}{\partial U}$$
$$B_{15,AERO} = \frac{\partial T_0(U)}{\partial U}z_d \tag{4}$$

Similarly, the aerodynamic pitch moment on the floating wind turbine is

$$X_{5,AERO} = T_0(U)z_d \tag{5}$$

while the damping coefficients are

$$B_{51,AERO} = \frac{\partial T_0(U)}{\partial U} z_d$$

$$B_{55,AERO} = \frac{\partial T_0(U)}{\partial U} z_d^2$$

(6)

In the present study, the aerodynamic thrust is approximated by the actuator disc concept:

$$T_0(U) = 2\rho_{AIR}A_d U^2 a(1-a)$$

(7)

where A_d is the area of the actuator disk and a is called the *axial flow induction factor*, which has been tuned to yield a similar result as that from the NREL wind turbine simulator FAST (Fatigue, Aerodynamics, Structures, and Turbulence).

For the case where the wind direction is taken to be the same as that of the incident waves, the aerodynamic loading is

$$X_{1,AERO} = 2\rho_{AIR}A_d U^2 a(1-a)\cos\beta$$

$$X_{2,AERO} = 2\rho_{AIR}A_d U^2 a(1-a)\sin\beta$$

$$X_{4,AERO} = -2\rho_{AIR}A_d U^2 a(1-a)z_d \sin\beta$$

$$X_{5,AERO} = 2\rho_{AIR}A_d U^2 a(1-a)z_d \cos\beta$$

(8)

while the damping coefficients are

$$B_{11,AERO} = 4\rho_{AIR}A_d U a(1-a)\cos\beta$$

$$B_{15,AERO} = 4\rho_{AIR}A_d U a(1-a)z_d \cos\beta$$

$$B_{51,AERO} = 4\rho_{AIR}A_d U a(1-a)z_d \cos\beta$$

$$B_{55,AERO} = 4\rho_{AIR}A_d U a(1-a)z_d^2 \cos\beta$$

$$B_{22,AERO} = 4\rho_{AIR}A_d U a(1-a)\sin\beta$$

$$B_{24,AERO} = 4\rho_{AIR}A_d U a(1-a)z_d \sin\beta$$

$$B_{42,AERO} = 4\rho_{AIR}A_d U a(1-a)z_d \sin\beta$$

$$B_{44,AERO} = 4\rho_{AIR}A_d U a(1-a)z_d^2 \sin\beta$$

(9)

Aerodynamic loading or damping in the heave or yaw modes of motion are neglected.

Appendix C

Time-domain Calculation

The responses of the floating wind turbines to nonlinear wave excitation are evaluated in the time-domain by solving the equations of motion:

$$(\mathbf{M} + \mathbf{A})\ddot{\xi} + \mathbf{B}\dot{\xi} + \mathbf{C}\xi = \mathbf{X}(t) \tag{1}$$

C.1 Calculation of the Coefficients

This section develops expressions for the added mass matrix $\mathbf{A}$ and the damping matrix $\mathbf{B}$. The mass matrix $\mathbf{M}$ and the restoring matrix $\mathbf{C}$ are the same as that computed by SWIM in the linear frequency-domain analysis in Chapter 3.

C.1.1 Added Mass Coefficients

All added mass coefficients are estimated by their zero-frequency values. The coefficients are

$$A_{11} \cong \pi\rho r^2 T + 4.754\rho\left(\tfrac{b}{2}\right)^2 (2 \times 0.866L)$$

$$A_{22} \cong \pi\rho r^2 T + 4.754\rho\left(\tfrac{b}{2}\right)^2 (2 \times 0.5L + L)$$

$$A_{33} \cong \tfrac{4}{3}\pi\rho r^3 \times 0.63 + 3 \times 4.754\rho\left(\tfrac{b}{2}\right)^2 L$$

$$A_{44} \cong \pi\rho r^2 \tfrac{T^3}{3} + 4.754\rho T^2\left(\tfrac{b}{2}\right)^2 (2 \times 0.5L + L)$$

$$A_{55} \cong \pi\rho r^2 \tfrac{T^3}{3} + 4.754\rho T^2\left(\tfrac{b}{2}\right)^2 (2 \times 0.866L) \tag{2}$$

$$A_{51} \cong A_{15} \cong \pi\rho r^2 \tfrac{T^2}{2} + 4.754\rho T\left(\tfrac{b}{2}\right)^2 (2 \times 0.866L)$$

$$A_{42} \cong A_{24} \cong -\pi\rho r^2 \tfrac{T^2}{2} - 4.754\rho T\left(\tfrac{b}{2}\right)^2 (2 \times 0.5L + L)$$

$$A_{66} \cong 3 \times 4.754\rho\left(\tfrac{b}{2}\right)^2\left(-\tfrac{r^3}{3} + \tfrac{(L+r)^3}{3}\right)$$

All other $A_{ij} = 0$

where L is the length of each radial arm and b is the breadth/height of the cross-section. For the case of *Design #2a*, $L = 0$, and the second term of each expression disappears. Furthermore, there is no added mass in yaw for the case of *Design #2a*.

C.1.2 Wave Damping

The diagonal terms of the damping matrix **B** can be approximated by the Haskind relations:

$$B_{ii} = \frac{k}{8\pi\rho g V_g} \int_0^{2\pi} |X_i(\theta)|^2 d\theta \qquad (3)$$

where V_g is the group velocity of the incident waves and X is the excitation. For an axisymmetric body, then,

$$B_{11} = \frac{k|X_1/_A|^2}{8\pi\rho g V_g} \int_0^{2\pi} \cos^2\theta d\theta = \frac{k|X_1/_A|^2}{8\rho g V_g}$$

$$B_{22} = \frac{k|X_2/_A|^2}{8\pi\rho g V_g} \int_0^{2\pi} \cos^2\theta d\theta = \frac{k|X_2/_A|^2}{8\rho g V_g}$$

$$B_{33} = \frac{k|X_3/_A|^2}{8\pi\rho g V_g} \int_0^{2\pi} d\theta = \frac{k|X_3/_A|^2}{4\rho g V_g} \qquad (4)$$

$$B_{44} = \frac{k|X_4/_A|^2}{8\pi\rho g V_g} \int_0^{2\pi} \cos^2\theta d\theta = \frac{k|X_4/_A|^2}{8\rho g V_g}$$

$$B_{55} = \frac{k|X_5/_A|^2}{8\pi\rho g V_g} \int_0^{2\pi} \cos^2\theta d\theta = \frac{k|X_5/_A|^2}{8\rho g V_g}$$

C.2 Calculation of the Viscous Drag Forces and Moments

The viscous drag forces (due to flow separation) upon the floating buoy may be expressed as follows:

$$dX_{1,VISCOUS,BUOY} = \tfrac{1}{2}\rho C_D d|u - \dot\xi_1|(u - \dot\xi_1)dz$$

$$dX_{2,VISCOUS,BUOY} = \tfrac{1}{2}\rho C_D d|v - \dot\xi_2|(v - \dot\xi_2)dz \qquad (5)$$

where d is the platform diameter and C_D is the drag coefficient of a 2-D circular cylinder. Assuming that $|u| \ll |\dot\xi_1|$ and $|v| \ll |\dot\xi_2|$, integrating across the draft, T, of the floating platform gives

$$X_{1,VISCOUS,BUOY} \cong -\tfrac{1}{2}\rho C_D dT|\dot\xi_1|\dot\xi_1$$

$$X_{2,VISCOUS,BUOY} \cong -\tfrac{1}{2}\rho C_D dT|\dot\xi_2|\dot\xi_2 \qquad (6)$$

In the same way, the viscous drag moments upon the floating buoy may be expressed as

$$X_{4,VISCOUS,BUOY} \cong \int_{-T}^{0} \frac{1}{2}\rho C_D d \left| z\dot{\xi}_4 \right| z\dot{\xi}_4(-z)dz$$

$$= \frac{1}{2}\rho C_D d \int_{-T}^{0} |z| \left| \dot{\xi}_4 \right| z\dot{\xi}_4(-z)dz$$

$$= -\frac{1}{2}\rho C_D d \left| \dot{\xi}_4 \right| \dot{\xi}_4 \int_{-T}^{0} |z| z^2 dz \qquad (7)$$

$$= -\frac{1}{2}\rho C_D d \left| \dot{\xi}_4 \right| \dot{\xi}_4 \int_{-T}^{0} (-z^3) dz$$

$$= -\frac{1}{2}\rho C_D d \left| \dot{\xi}_4 \right| \dot{\xi}_4 \frac{T^4}{4}$$

$$X_{5,VISCOUS,BUOY} \cong -\int_{-T}^{0} \frac{1}{2}\rho C_D d \left| z\dot{\xi}_5 \right| z\dot{\xi}_5(z)dz$$

$$= -\frac{1}{2}\rho C_D d \int_{-T}^{0} |z| \left| \dot{\xi}_5 \right| z^2 \dot{\xi}_5 dz$$

$$= -\frac{1}{2}\rho C_D d \left| \dot{\xi}_5 \right| \dot{\xi}_5 \int_{-T}^{0} |z| z^2 dz \qquad (8)$$

$$= -\frac{1}{2}\rho C_D d \left| \dot{\xi}_5 \right| \dot{\xi}_5 \int_{-T}^{0} (-z^3) dz$$

$$= -\frac{1}{2}\rho C_D d \left| \dot{\xi}_5 \right| \dot{\xi}_5 \frac{T^4}{4}$$

Adding the contribution due to the radial arms, the total viscous drag forces and moments become

$$X_{1,VISCOUS} \cong -\frac{1}{2}\rho C_D dT \left| \dot{\xi}_1 \right| \dot{\xi}_1 - \frac{1}{2}\rho C_{D,square} b(2 \times 0.886L) \left| \dot{\xi}_1 \right| \dot{\xi}_1$$

$$X_{2,VISCOUS} \cong -\frac{1}{2}\rho C_D dT \left| \dot{\xi}_2 \right| \dot{\xi}_2 - \frac{1}{2}\rho C_{D,square} b(2 \times 0.5L + L) \left| \dot{\xi}_2 \right| \dot{\xi}_2$$

$$X_{4,VISCOUS} \cong -\frac{1}{2}\rho C_D d \left| \dot{\xi}_4 \right| \dot{\xi}_4 \frac{T^4}{4} - \frac{1}{2}\rho C_{D,square} b(2 \times 0.5L + L)T^3 \left| \dot{\xi}_4 \right| \dot{\xi}_4 \qquad (9)$$

$$X_{5,VISCOUS} \cong -\frac{1}{2}\rho C_D d \left| \dot{\xi}_5 \right| \dot{\xi}_5 \frac{T^4}{4} - \frac{1}{2}\rho C_{D,square} b(2 \times 0.886L)T^3 \left| \dot{\xi}_5 \right| \dot{\xi}_5$$

where $C_{D,square}$ is the drag coefficient of a square section. Finally, the viscous drag force and moment in heave and yaw are

$$X_{3,VISCOUS} = -\tfrac{1}{2}\rho C_{D,square}(3bL)\left|\dot{\xi}_3\right|\dot{\xi}_3$$

$$X_{6,VISCOUS} \cong -3 \int_{r}^{r+L} \tfrac{1}{2}\rho C_{D,square} b \left|x\dot{\xi}_6\right| x\dot{\xi}_6(x)dx$$

$$= -\tfrac{3}{2}\rho C_{D,square} b \int_{r}^{r+L} \left|x\right|\left|\dot{\xi}_6\right| x^2\dot{\xi}_6 dx$$

$$= -\tfrac{3}{2}\rho C_{D,square} b \left|\dot{\xi}_6\right|\dot{\xi}_6 \int_{r}^{r+L} \left|x\right| x^2 dx$$

$$= -\tfrac{3}{2}\rho C_{D,square} b \left|\dot{\xi}_6\right|\dot{\xi}_6 \int_{r}^{r+L} x^3 dx$$

$$= -\tfrac{3}{8}\rho C_{D,square} b \left|\dot{\xi}_6\right|\dot{\xi}_6 \left[(r+L)^4 - r^4\right]$$

(10)

In all cases, frictional drag is neglected.

The equations of motion for the floating wind turbine (1) are then solved in the time-domain, where the excitation, $\mathbf{X}(t)$, is composed of the following:

$$X_i(t) = X_{i,WAVE}(t) + X_{i,VISCOUS}(t)$$

(11)

Bibliography

[1] Burton, T., Sharpe, D., Jenkins, N., and Bossanyi, E. *Wind Energy Handbook*. New York, NY: John Wiley and Sons, 2001.

[2] Chryssostomidis, C. and Triantafyllou, M.S. *Environment Description, Force Prediction, and Statistics for Design Applications in Ocean Engineering*, 1980.

[3] Grue, J. and Huseby, M. Higher-harmonic Wave Forces and Ringing of Vertical Cylinders. *Applied Ocean Research*, volume 24, 203-214, 2002.

[4] Kim, S. and Sclavounos, P.D. Fully Coupled Response Simulations of Theme Offshore Structures in Water Depths of Up to 10,000 Feet. *Proceedings of the Eleventh International Offshore and Polar Engineering Conference*, 2001.

[5] McCormick, M. E. *Anchoring Systems*. U.K.: Pergamon Press, 1979.

[6] Musial, W., Butterfield, S., and Boone, A. Feasibility of Floating Platform Systems for Wind Turbines. *23rd ASME Wind Energy Symposium*, 2004.

[7] Newman, J. N. *Marine Hydrodynamics*. Cambridge, MA: MIT Press, 1977.

[8] *Recommended Practice for Design and Analysis of Stationkeeping Systems for Floating Structures*, American Petroleum Institute, 1996.

[9] Sclavounos, P. D. Nonlinear Kinematics of Fluid Particles on the Surface of Stochastic Ocean Waves, 2004.

[10] Sclavounos, P. D. *13.022 Surface Waves and their Interaction with Floating Bodies Lecture Notes*, Massachusetts Institute of Technology, 2003.

[11] Tong, K. C. Technical and Economic Aspects of a Floating Offshore Wind Farm. *Journal of Wind Engineering and Industrial Aerodynamics*, 74-76, 1998.

[12] Williams, Jr., J. H. *Fundamentals of Applied Dynamics*. New York, NY: John Wiley & Sons, Inc., 1996.

[13] Withee, E. Fully Coupled Dynamic Analysis of a Floating Wind Turbine System, Unpublished doctoral thesis, Massachusetts Institute of Technology, 2004.